Exact holographic RG flows and the A1 x A1 Toda chain

Irina Ya. Aref'eva, Anastasia Golubtsova, Giuseppe Policastro

JHEP

Published for SISSA by Springer

Received: January 25, 2019
Accepted: April 2, 2019
Published: May 21, 2019

Exact holographic RG flows and the $A_1 \times A_1$ Toda chain

Irina Ya. Aref'eva,[a] **Anastasia A. Golubtsova**[b,c] **and Giuseppe Policastro**[d]

[a] *Steklov Mathematical Institute, Russian Academy of Sciences, Gubkina str. 8, Moscow, 119991 Russia*

[b] *Bogoliubov Laboratory of Theoretical Physics, Joint Institute for Nuclear Research, Joliot-Curie str. 6, Dubna, 141980 Russia*

[c] *Dubna State University, Universitetskaya str. 19, Dubna, 141980 Russia*

[d] *Laboratoire de Physique Théorique de l'École Normale Supérieure, PSL University, CNRS, Sorbonne Universités, UPMC Université Paris 06, 24 rue Lhomond, Paris Cedex 05, 75231 France*

E-mail: arefeva@mi.ras.ru, golubtsova@theor.jinr.ru, policast@lpt.ens.fr

Abstract: We construct analytic solutions of Einstein gravity coupled to a dilaton field with a potential given by a sum of two exponentials, by rewriting the equations of motion in terms of an integrable Toda chain. These solutions can be interpreted as domain walls interpolating between different asymptotics, and as such they can have interesting applications in holography. In some cases, we can construct a solution which interpolates between an AdS fixed point in the UV limit and a hyperscaling violating boundary in the IR region. We also find analytic black brane solutions at finite temperature. We discuss the properties of the solutions and the interpretation in terms of RG flow.

Keywords: Gauge-gravity correspondence, Holography and quark-gluon plasmas, AdS-CFT Correspondence

ArXiv ePrint: 1803.06764v2

https://doi.org/10.1007/JHEP05(2019)117

JHEP05(2019)117

Contents

JHEP05(2019)117

1 Introduction

The notion of the renormalization group has dominated our thinking about quantum field theories and statistical systems since its elaboration by K. Wilson. It has been a paradigm-changing idea, providing a unified and systematic picture to understand the dynamics of systems with many degrees of freedoms. Quantum field theories are now not seen as isolated items, but as classes connected by the RG flow. The method is very powerful, however in practice one can usually only determine the structure of the flow in a perturbative expansion around a fixed point that is weakly coupled. Luckily there are many interesting theories for which the program can be implemented, including of course Yang-Mills and QCD that are asymptotically free, the Wilson-Fisher fixed point of $\lambda\phi^4$ in dimension $4-\epsilon$, etc., but strongly-coupled examples are few.

The holographic correspondence gives a description of a class of strongly-coupled field theories in terms of a dual weakly-coupled gravitational description. The RG flow in this description is geometrized, and corresponds to a gravitational solution with particular asymptotic properties; the holographic direction corresponds to the energy scale, and so the Hamiltonian evolution in this direction can be put in correspondence with the evolution of the system under the change of the RG scale [1]. These solutions are often described as "domain wall" solutions, as they interpolate between two asymptotic regions, each of them being a solution on its own and corresponding to a given theory [2]–[4].

This aspect of the holographic correspondence has been intensely explored, but some issues have so far eluded a complete resolution; for instance, the precise relation between the holographic and the Wilsonian scheme [5, 6], and the fact that Einstein equations are second order while RG equations are first-order; even though the equations can be cast in first-order form using the Hamilton-Jacobi formalism, there seems still to be a mismatch in that the couplings of the field theory are promoted to fluctuating fields in the gravity description; recently an attempt to solve this problem has been made [7] with the notion of a "quantum RG flow", that arises from the classical one after integrating out the double-trace operators. This flow may be more complex than the one typically arising in QFT, and these possibilities have only been considered in the last few years [8].

The matching of RG equations with the gravity equations has been precisely formulated only for the solutions that have the Poincaré invariance at the boundary, and correspond to the vacuum of the dual field theory. In these cases, one can show that the equations of motion can be expressed in terms of a superpotential, which is determined by the scalar potential (up to the choice of some integration constants), and is in one-to-one correspondence with the beta function of the dual theory. But it is not yet known how to extend this procedure to non-Poincaré invariant states, in particular finite temperature/density.

In this paper we will not be concerned with these conceptual issues. Rather, in the spirit of "bottom-up" holography, we remark that there are some relatively simple models of gravity coupled to a scalar field, that allow for interesting examples of RG flows that can be found analytically. This is due to the fact that the Einstein equations, with the Ansatz that corresponds to domain-walls solutions, reduce to dynamical equations that are completely integrable (they can be reduced to the equations of a Toda chain). It is

JHEP05(2019)117

remarkable that such analytic domain-wall solutions can be found not only for the vacuum but also at finite temperature. The Toda equations arise when the potential is a sum of exponentials, when the coefficients in the exponent satisfy certain relations. The case of a single exponential term had been solved in [9]. The Chamblin-Reall black brane solution has found applications to the study of the dynamics of a non-conformal strongly coupled plasma in the hydro regime and beyond [10, 11]. However the single exponential case has some limitations: the potential is monotonous, so it does not have a minimum but only run-away solutions; the RG flow in this case does not start from a UV fixed point, and in fact the dual theory is not well-behaved in the UV. Moreover, the single exponential has a definite sign. This precludes the possibility of studying cases in which the potential changes sign along the solution. The general analysis of RG flow with a single scalar, performed in [8], only deals with potentials that are definite negative; the general case of a potential with zeros is less explored.

In this paper we consider the next simplest case, with a sum of two exponentials. Integrability leaves one of the two exponents unfixed, so we have one free parameter, like in the case of a single exponential. This case already allows to overcome the limitations just mentioned. We will leave the consideration of more complicated potentials for future investigations. Qualitatively, the properties of the potential is that it has a minimum with $V_{\min} < 0$, it goes from being negative and vanishing at $\phi \to -\infty$ to positive and diverging at $\phi \to +\infty$.

It turns out that for our choice of the potential, the integrable Toda chain is associated to the Lie algebra is $A_1 \times A_1$ [12, 13], so it is a particularly simple case and the solutions can be given explicitly in terms of elementary functions.

The solutions we find depend on a certain number of parameters. One parameter distinguishes between vacuum and nonvacuum solutions. The vacuum solutions are Poincaré invariant. Turning on the parameter gives a deformation to non-vacuum solutions, in which Poincaré symmetry is broken, and horizons can be formed. One more constant is the "energy" of the solutions (more exactly the energy in the associated Toda chain description) and determines the type of solutions; there are four general classes of solutions — depending on the type of functions that appear, we will call them the sinh-class, sin-class, linear class and cosh-class of solutions (see eqs. (2.33)). We will consider mainly the sinh-class. Two other parameters determine the position of singularities, whose presence requires to split the domain on the radial variable in three regions; correspondingly we have "left", "middle" and "right" solutions. In the left and middle solutions the dilaton interpolates between $+\infty$ and $-\infty$, whereas the right solution is bouncing: the dilaton starts at $-\infty$, goes to a maximal value and then goes back to $-\infty$. It should be noted that the singularities are not just coordinate singularities; the scalar curvature usually diverges at the end points of the branches, except for the right end of the middle branch.

Coming to the domain wall coordinates we explore the solutions in the holographic framework. We define the energy scale $\mathrm{A} = e^{\mathcal{A}}$, where $\mathcal{A}$ is the scale factor of the domain wall metric and the running coupling as $\lambda = e^{\phi}$ through the dilaton ϕ. It is interesting that, in spite of the fact that the dilaton has a similar behaviour in the left and middle solutions, the scale factor $\mathcal{A}$ has rather different behaviour on these solutions, namely, on the left

JHEP05(2019)117

solution when the dilaton varies from $-\infty$ to a special value ϕ_s, the energy scale increases, but after the dilaton passes the special value ϕ_s, the scale factor starts to decrease down. This non-monotonic behavior of $\mathcal{A}$ precludes the possibility of a holographic interpretation of this branch of solutions. For the middle solution, when the dilaton increases from $-\infty$ to ∞, the scale factor decreases from large positive values to large negative values. This behaviour corresponds to the running coupling in an asymptotically UV free theory, so it is of interest from the point of view of possible applications in QCD. In the right solution the scale factor is increasing from minus infinity to plus infinity, but the dilaton bounces back after reaching a maximal value $\phi_{\max}$, as already mentioned. These behaviours are illustrated in figure 8.

There is also a special case when the points of singularities coincide. In this case the singularities are cancelled and the solution has a smooth AdS boundary in the UV limit and a hyperscaling violating boundary in the IR region. The dilaton supporting this geometry runs from a constant value in the UV to $-\infty$ in the IR.

As we mentioned before there are other solutions, in particular this one from the linear class describes the opposite flow, from hyperscaling-violating in the UV to AdS in the IR.

When we turn to non-vacuum solutions, the deformation can give solutions with a horizon or without. For the cases having horizons, the parameter characterizing the deformation is related to the temperature. It happens that the black brane solutions can be constructed only from those vacuum solutions which are defined for $u \to \pm\infty$. For these solutions the dilaton potential evaluated on-shell is bounded from above and therefore the solutions obey Gubser's criterion [22]. In particular, for the solutions defined for $u \to +\infty$ we change the scaling properties of these solutions in the IR regime varying the temperature, meanwhile the UV behavior does not change.

In accordance with Gubser's criterion, we find finite temperature solutions only for the "regular" vacuum flow. In particular, we do not have any black brane solution with AdS UV asymptotics, as this is a singular flow. The finite temperature generalization of the vacuum solution with coinciding singularities yields to be just a AdS-Schwarzschild black brane, i.e. it does not flow anymore.

The interpretation of the solutions in terms of RG flows is clarified by using the first order variables X, Y [14] that have a direct relation to the superpotential and the beta function, when a dual theory interpretation is possible. We discuss how our solutions describe flows between different attractor points in the phase space, i.e. the (ϕ, X) plane, but in order to recover all possible flows we also have to include other classes of solutions, namely the linear and cosh-solutions. This is illustrated in figures 9 and 10. In figure 16 we show possible flows at non-zero temperature.

The paper is organized as follows. In section 2 we describe the holographic gravity model, the ansatz for the metric and the dilaton that leads to a special mechanical model, that can be explicitly integrated. Here (section 2.5) we also introduce some general relations for the holographic RG flow. In section 3 we describe in details the vacuum solutions and give their interpretation in terms of the holographic RG flow. In section 4 we study non-vacuum solutions, derive a black brane and study the black brane solution as a holographic RG flow at finite temperature. In the appendix, we collect information about curvature

JHEP05(2019)117

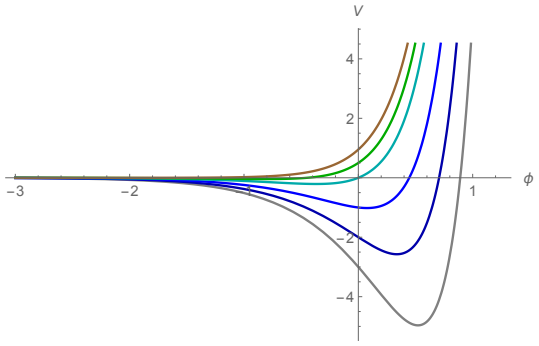

Figure 1. The behaviour of the potential $V(\phi)$ for $C_1 < 0$, $C_2 > 0$.

invariants for our background in section A, some formula about the dilaton field in section B and details about the superpotential for vacuum case in section C.

2 The setup

We consider a holographic model with gravity coupled to a dilaton field, and the dilaton potential is taken as a sum of two exponential functions. As explained in the introduction, the choice of the dilaton potential is motivated by studies of models with only one exponential function in the potential [10, 14].

2.1 The holographic gravity model

The holographic model is governed by an action of the form

$$\mathcal{S} = \frac{1}{16\pi G_5}\int d^5x\sqrt{|g|}\left(R - \frac{4}{3}(\partial\phi)^2 - V(\phi)\right) + G.H., \tag{2.1}$$

with the dilaton potential

$$V(\phi) = C_1 e^{2k_1\phi} + C_2 e^{2k_2\phi}, \tag{2.2}$$

where C_i, k_i with $i = 1, 2$ are constants. We choose the constants C_1 and C_2 as follows

$$C_1 < 0, \quad C_2 > 0. \tag{2.3}$$

In this case the potential has a minimum and regions of positive and negative sign, as shown in figure 1.

The model (2.1)–(2.2) is defined on a 5-dim manifold M equipped with the metric

$$ds^2 = -e^{2A(u)}dt^2 + e^{2B(u)}\sum_{i=1}^{3} dy_i^2 + e^{2C(u)}du^2, \tag{2.4}$$

where $A = A(u)$, $B = B(u)$ and $C = C(u)$ are some smooth functions. We make an ansatz in which these functions, as well as the dilaton, depend only on the u-coordinate.

The equations of motion which follow from the action (2.1) read

$$R_{MN} - \frac{1}{2}g_{MN}R = \frac{4}{3}\left(\partial_M\phi\partial_N\phi - \frac{1}{2}g_{MN}\partial_k\phi\partial^k\phi\right) - \frac{1}{2}g_{MN}V(\phi). \tag{2.5}$$

JHEP05(2019)117

The equation for the scalar field is

$$\Box\phi = \frac{3}{8}\frac{\partial V}{\partial \phi}. \tag{2.6}$$

Taking into account the relations (A.2)–(A.6), (B.1), the Lagrangian can be reduced to the following form, up to total derivative terms:

$$L = \frac{1}{2}\left[-e^{A+3B-C}(6\dot{A}\dot{B} + 6\dot{B}^2) + \frac{4}{3}\dot{\phi}^2 e^{A+3B-C} + e^{A+3B+C}V(\phi)\right], \tag{2.7}$$

where we denote $\dot{} \equiv \frac{d}{du}$. For convenience we redefine the functions as

$$A(u) = x^1(u), \quad B(u) = x^2(u), \quad \phi(u) = x^3(u), \quad C(u) = x(u), \tag{2.8}$$

introduce a new variable x_0

$$x_0 = x^1 + 3x^2 \tag{2.9}$$

and the so-called lapse function

$$\mathcal{N} = e^{x-x_0}. \tag{2.10}$$

In what follows we use the harmonic gauge, i.e.

$$\mathcal{N} = 1, \quad \text{or} \quad x = x_0. \tag{2.11}$$

The explicit form of E.O.M. is presented in appendix A.1 in the harmonic gauge $C = A + 3B$.

2.2 Mechanical model

The Lagrangian (2.7) with the help of (2.8)–(2.11) can be taken to the following form (see [21] and refs. therein)

$$L = \frac{1}{2}G_{ij}\dot{x}^i\dot{x}^j - V(x), \tag{2.12}$$

$$V = -\frac{1}{2}\sum_{s=1}^{2} C_s e^{2(x^1+3x^2+k_s x^3)}, \tag{2.13}$$

where the minisupermetric G_{ij} on the target space $\mathcal{M}$ reads

$$(G_{ij}) = \begin{pmatrix} 0 & -3 & 0 \\ -3 & -6 & 0 \\ 0 & 0 & \frac{4}{3} \end{pmatrix}, \quad (G^{ij}) = \begin{pmatrix} \frac{2}{3} & -\frac{1}{3} & 0 \\ -\frac{1}{3} & 0 & 0 \\ 0 & 0 & \frac{3}{4} \end{pmatrix}, \quad i,j = 1,2,3. \tag{2.14}$$

The corresponding energy constraint is given by

$$E = \frac{1}{2}G_{ij}\dot{x}^i\dot{x}^j + V = 0. \tag{2.15}$$

However, the system (2.12)–(2.15) is still difficult to work with, because of the degrees of freedom are coupled in the potential. The idea of the next section is to separate the equations of motion rotating the system [18, 19].

JHEP05(2019)117

2.3 Integration of the mechanical model

To perform the following calculations it is useful to present the mechanical Lagrangian (2.12) in the form

$$L = \frac{1}{2}\langle \dot{x}, \dot{x} \rangle + \frac{C_1}{2} e^{\langle V, x \rangle} + \frac{C_2}{2} e^{\langle W, x \rangle}, \tag{2.16}$$

where V and W are some vectors on the target space (we suppose that the original basis is (e_1, e_2, e_3)), the brackets denote a scalar product on the target space $\mathcal{M}$ with the metric (2.14).

Then the components of V and W are defined by

$$V^1 = -\frac{2}{3}, \quad V^2 = -\frac{2}{3}, \quad V^3 = \frac{3}{2}k_1, \tag{2.17}$$

$$W^1 = -\frac{2}{3}, \quad W^2 = -\frac{2}{3}, \quad W^3 = \frac{3}{2}k_2. \tag{2.18}$$

The method we will use applies generally to systems with interactions of the form (2.16), with arbitrarily many exponentials [18–20]. It turns out that the system is integrable if the vectors V and W can be identified with the root vectors of a Lie algebra (for more details see [12, 13, 18, 19]). Then the system becomes a Toda chain. In our case, we can see that the scalar products of the vectors are:

$$\langle V, V \rangle = 3\left(k_1^2 - \frac{16}{9}\right), \quad \langle W, W \rangle = 3\left(k_2^2 - \frac{16}{9}\right), \quad \langle V, W \rangle = 3\left(k_1 k_2 - \frac{16}{9}\right). \tag{2.19}$$

These correspond to the roots of a Lie algebra only if V and W are orthogonal, in which case we have the $A_1 \times A_1$ Toda model. The integrability requirement puts a restriction on the dilaton couplings:

$$\langle V, W \rangle = 0, \quad k_1 k_2 = \frac{16}{9}. \tag{2.20}$$

We also suppose that V is a timelike vector and W is a spacelike one (notice that the symmetry between k_1 and k_2 is broken by the choice of the signs of the coefficients in the potential). We rename

$$k_1 = k, \quad k_2 = \frac{16}{9k}, \tag{2.21}$$

and we have the condition

$$0 < k < 4/3. \tag{2.22}$$

We can find a basis of orthonormal vectors with respect to the metric G_{ij}:

$$\left\langle e_i^{'}, e_j^{'} \right\rangle = \eta_{ij}, \quad \text{with} \quad (\eta_{ij}) = \text{diag}\,(-1, 1, 1), \quad i, j = 1, 2, 3; \tag{2.23}$$

one can choose the new basis vectors as follows

$$e_1^{'} = \frac{V}{||V||}, \quad e_2^{'} = \frac{W}{||W||}. \tag{2.24}$$

JHEP05(2019)117

The new basis is related to the old one by a Lorentz transformation:

$$e_j^{'} = \sum_{i=1}^{3} S_j^i e_i, \quad \sum_{k,l=1}^{3} G_{kl} S_i^k S_j^l = \eta_{ij}, \tag{2.25}$$

and the coordinates transform as

$$x^i = \sum_{j=1}^{3} S_j^i X^j, \quad X^i = \eta_{ii} \left\langle e_i^{'}, x \right\rangle . \tag{2.26}$$

The Lagrangian and the energy constraint (2.12)–(2.15) in the new basis take the form

$$L = \frac{1}{2} \sum_{i,j=1}^{3} \eta_{ij} \dot{X}^i \dot{X}^j + \frac{C_1}{2} \exp\left[\eta_{11} |\langle V, V \rangle|^{1/2} X^1\right] + \frac{C_2}{2} \exp\left[\eta_{22} |\langle W, W \rangle|^{1/2} X^2\right], \tag{2.27}$$

$$E_0 = \frac{1}{2} \sum_{i,j=1}^{3} \eta_{ij} \dot{X}^i \dot{X}^j - \frac{C_1}{2} \exp\left[\eta_{11} |\langle V, V \rangle|^{1/2} X^1\right] - \frac{C_2}{2} \exp\left[\eta_{22} |\langle W, W \rangle|^{1/2} X^2\right]. \tag{2.28}$$

From (2.27)–(2.28) we see that mechanical variables are decoupled, so the equations of motion following from the Lagrangian (2.27) are

$$\ddot{X}^s = |\langle R_s, R_s \rangle|^{1/2} \frac{C_s}{2} \exp\left[\eta_{ss} |\langle R_s, R_s \rangle|^{1/2} X^s\right], \tag{2.29}$$

$$\ddot{X}^3 = 0, \tag{2.30}$$

where $s = 1, 2$ and we introduce a notation for the scalar product

$$\langle R_1, R_1 \rangle = \langle V, V \rangle , \qquad \langle R_2, R_2 \rangle = \langle W, W \rangle . \tag{2.31}$$

The eqs. (2.29) with $s = 1, 2$ are two decoupled Liouville equations. The solution can be given explicitly:

$$X^s = -\eta_{ss} |\langle R_s, R_s \rangle|^{-1/2} \ln\left(F_s^2 (u - u_{0s})\right), \tag{2.32}$$

with the functions

$$F_s(u - u_{0s}) = \begin{cases} \sqrt{\dfrac{|C_s|}{2|E_s|}} \sinh\left[\sqrt{\dfrac{|E_s \langle R_s, R_s \rangle|}{2}} (u - u_{0s})\right], & \text{if} \quad \eta_{ss} C_s > 0, \quad \eta_{ss} E_s > 0, \\ \sqrt{\dfrac{|C_s|}{2|E_s|}} \sin\left[\sqrt{\dfrac{|E_s \langle R_s, R_s \rangle|}{2}} (u - u_{0s})\right], & \text{if} \quad \eta_{ss} C_s > 0, \quad \eta_{ss} E_s < 0, \\ \sqrt{\dfrac{|\langle R_s, R_s \rangle C_s|}{4}} (u - u_{0s}), & \text{if} \quad \eta_{ss} C_s > 0, \quad E_s = 0, \\ \sqrt{\dfrac{|C_s|}{2|E_s|}} \cosh\left[\sqrt{\dfrac{|E_s \langle R_s, R_s \rangle|}{2}} (u - u_{0s})\right], & \text{if} \quad \eta_{ss} C_s < 0, \quad \eta_{ss} E_s > 0, \end{cases} \tag{2.33}$$

JHEP05(2019)117

where u_{0s}, E_s are constants of integration, $s = 1, 2$. The E_s are the conserved energies of the two decoupled Liouville modes. In our case, with $C_1 < 0$ and $C_2 > 0$, we have $\eta_{ss} C_s > 0$, so the relevant solutions are given by the first three lines. We will analyze in detail the sinh-solutions, which are the most interesting from the RG point of view.

The solutions to eq. (2.30) is

$$X^3 = p^3 u + q^3, \tag{2.34}$$

with constants of integration p^3, q^3.

Having solved the system, we can go back to the original variables applying the transformations (2.26) with components

$$S_1^i = \frac{V^i}{|\langle V, V\rangle|^{1/2}}, \quad S_2^i = \frac{W^i}{\langle W, W\rangle^{1/2}}, \tag{2.35}$$

and obtain

$$\exp x^1 = [F_1(u-u_{01})]^{-\frac{2V^1}{\langle V,V\rangle}} [F_2(u-u_{02})]^{-\frac{2W^1}{\langle W,W\rangle}} e^{\alpha^1 u+\beta^1}, \tag{2.36}$$

$$\exp x^2 = [F_1(u-u_{01})]^{-\frac{2V^2}{\langle V,V\rangle}} [F_2(u-u_{02})]^{-\frac{2W^2}{\langle W,W\rangle}} e^{\alpha^2 u+\beta^2}, \tag{2.37}$$

$$\exp x^3 = [F_1(u-u_{01})]^{-\frac{2V^3}{\langle V,V\rangle}} [F_2(u-u_{02})]^{-\frac{2W^3}{\langle W,W\rangle}} e^{\alpha^3 u+\beta^3}, \tag{2.38}$$

with the parameters α^i, β^i defined using (2.25)

$$\alpha^i = S_3^i p^3, \quad \beta^i = S_3^i q^3. \tag{2.39}$$

The parameters α^i satisfy the following conditions

$$\langle \alpha, V\rangle = 0, \quad \langle \alpha, W\rangle = 0, \tag{2.40}$$

which imply

$$\alpha^3 = 0, \quad \alpha^1 = -3\alpha^2\,. \tag{2.41}$$

The constants E_1, E_2 and α^i are related by the constraint (2.28) which reads

$$E_1 + E_2 + \frac{1}{2}\langle \alpha, \alpha\rangle = E_0\,. \tag{2.42}$$

2.4 The exact solutions in the harmonic gauge

Keeping in mind that the variables x^i with (2.36)–(2.38), (2.41) are redefined metric functions A, B and the dilaton ϕ (2.8)–(2.9), and taking the gauge condition $C = A+3B$ (2.11) into account, we can write down the metric coefficients of (2.4)

$$e^A = F_1^{\frac{4}{9k^2-16}} F_2^{\frac{9k^2}{4(16-9k^2)}} e^{\alpha^1 u}, \tag{2.43}$$

$$e^B = F_1^{\frac{4}{9k^2-16}} F_2^{\frac{9k^2}{4(16-9k^2)}} e^{-\frac{\alpha^1}{3} u}, \tag{2.44}$$

$$e^C = F_1^{\frac{16}{9k^2-16}} F_2^{\frac{9k^2}{16-9k^2}}, \tag{2.45}$$

JHEP05(2019)117

where for simplicity we put β^i, $i = 1, 2, 3$, to zero (without loss of generality, as this corresponds to a rescaling of the coordinates). For the dilaton we have

$$\phi = -\frac{9k}{9k^2-16}\log F_1 + \frac{9k}{9k^2-16}\log F_2, \tag{2.46}$$

moreover the dilaton equation (2.6) requires to take $E_0 = 0$ in (2.42), i.e.

$$E_1 + E_2 + \frac{2(\alpha^1)^2}{3} = 0, \tag{2.47}$$

with $E_1 < 0$, $E_2 > 0$ and the value of E_1 is bounded as $|E_1| = E_2 + \frac{2(\alpha^1)^2}{3}$.

Then the functions F_1 and F_2 in (2.43)–(2.46) are given by

$$F_1 = \sqrt{\left|\frac{C_1}{2E_1}\right|}\sinh(\mu_1|u-u_{01}|),\ \mu_1 = \sqrt{\left|\frac{3E_1}{2}\left(k^2-\frac{16}{9}\right)\right|}, \tag{2.48}$$

$$F_2 = \sqrt{\left|\frac{C_2}{2E_2}\right|}\sinh(\mu_2|u-u_{02}|),\ \mu_2 = \sqrt{\left|\frac{3E_2}{2}\left(\left(\frac{16}{9}\right)^2\frac{1}{k^2}-\frac{16}{9}\right)\right|}, \tag{2.49}$$

where $0 < k < 4/3$, C_1 and C_2 are given by (2.2)–(2.3). The generic form of the metric that solves EOM following from (2.1) reads

$$ds^2 = F_1^{\frac{8}{9k^2-16}}F_2^{\frac{9k^2}{2(16-9k^2)}}\left(-e^{2\alpha^1 u}dt^2 + e^{-\frac{2\alpha^1}{3}u}d\vec{y}^2\right) + F_1^{\frac{32}{9k^2-16}}F_2^{\frac{18k^2}{16-9k^2}}du^2, \tag{2.50}$$

where $\vec{y} = (y_1, y_2, y_3)$.

The dilaton potential evaluated on the solution becomes

$$V = C_1 e^{2k\phi} + C_2 e^{32\phi/(9k)} = C_1\left(\frac{F_2}{F_1}\right)^{\frac{18k^2}{9k^2-16}} + C_2\left(\frac{F_2}{F_1}\right)^{\frac{32}{9k^2-16}}. \tag{2.51}$$

We note that we have two more solutions for our choice of the potential (2.2) with $C_1 < 0$ and $C_2 > 0$ governed by F_1 and F_2 from the second and third branches of (2.33). The solutions differ by the range of integrating constants, i.e. for $E_1 > 0$ and $E_2 < 0$ (opposite signes to (2.48)–(2.49)), we have

$$F_1 = \sqrt{\left|\frac{C_1}{2E_1}\right|}\sin(\mu_1|u-u_{01}|), \qquad \mu_1 = \sqrt{\left|\frac{3E_1}{2}(k^2-\frac{16}{9})\right|}, \tag{2.52}$$

$$F_2 = \sqrt{\left|\frac{C_2}{2E_2}\right|}\sin(\mu_2|u-u_{02}|), \qquad \mu_2 = \sqrt{\left|\frac{3E_2}{2}\left(\left(\frac{16}{9}\right)^2\frac{1}{k^2}-\frac{16}{9}\right)\right|}, \tag{2.53}$$

while taking $E_1 = E_2 = 0$ one has

$$F_1 = \sqrt{\frac{3}{4}\left(k^2-\frac{16}{9}\right)C_1}(u-u_{01}), \quad F_2 = \sqrt{\frac{3}{4}\left(\left(\frac{16}{9k}\right)^2-\frac{16}{9}\right)C_2}(u-u_{02}). \tag{2.54}$$

JHEP05(2019)117

In the forth line of (2.33) we observe cosh-solutions for the functions F_1 and F_2

$$F_1 = \sqrt{\left|\frac{C_1}{2E_1}\right|}\cosh(\mu_1 |u-u_{01}|), \qquad \mu_1 = \sqrt{\left|\frac{3E_1}{2}(k^2-\frac{16}{9})\right|}, \tag{2.55}$$

$$F_2 = \sqrt{\left|\frac{C_2}{2E_2}\right|}\cosh(\mu_2 |u-u_{02}|), \qquad \mu_2 = \sqrt{\left|\frac{3E_2}{2}\left(\left(\frac{16}{9}\right)^2\frac{1}{k^2}-\frac{16}{9}\right)\right|}, \tag{2.56}$$

that corresponds to the dilaton potential with $C_1 > 0$, $C_2 < 0$ and integration constants $E_1 < 0$, $E_2 > 0$.

2.5 Solutions as RG flows

Let's briefly discuss the gravity solutions as holographic RG flows. It is useful to come to so-called domain wall coordinates. In this coordinates a general form of the non-vacuum solutions is

$$ds^2 = \frac{dw^2}{f(w)} + e^{2\mathcal{A}(w)}\left(-f(w)dt^2 + \delta_{ij}dx^i dx^j\right), \tag{2.57}$$

which covers the vacuum case with $f(w) = 1$. Both temperature and vacuum solutions are characterized by the scale factor $e^{\mathcal{A}(w)}$, that measures the field theory energy scale, the blackening function $f(w)$ and by a scalar field profile $\phi(w)$

$$\lambda = e^{\phi}, \tag{2.58}$$

which is interpreted as the running coupling.

If we define

$$X = \frac{1}{3\lambda}\frac{d\lambda}{d\mathcal{A}} \tag{2.59}$$

$$Y(\phi) = \frac{1}{4}\frac{g'}{\mathcal{A}'}, \quad g = \log f, \tag{2.60}$$

we get the system of first order differential equations

$$\frac{dX}{d\phi} = -\frac{4}{3}\left(1-X^2+Y\right)\left(1+\frac{3}{8X}\frac{d\log V}{d\phi}\right), \tag{2.61}$$

$$\frac{dY}{d\phi} = -\frac{4}{3}\left(1-X^2+Y\right)\frac{Y}{X}. \tag{2.62}$$

For the vacuum case we get

$$\frac{dX}{d\phi} = -\frac{4}{3}\left(1-X^2\right)\left(1+\frac{3}{8X}\frac{d\log V}{d\phi}\right). \tag{2.63}$$

JHEP05(2019)117

3 Vacuum solutions

3.1 The metric and the dilaton for vacuum exact solutions

The vacuum solutions are those that preserve the Poincaré invariance at the boundary. As can be seen from (2.50), this requires that $\alpha^1 = \alpha^2 = 0$, so in this case the two Liouville energies have to be:

$$|E_1| = |E_2|, \tag{3.1}$$

with the opposite signs $E_1 < 0$, $E_2 > 0$.

Owing to (3.1) the metric (2.50) takes the form

$$ds^2 = F_1^{\frac{8}{9k^2-16}} F_2^{\frac{9k^2}{2(16-9k^2)}} (-dt^2 + d\vec{y}^2) + F_1^{\frac{32}{9k^2-16}} F_2^{\frac{18k^2}{16-9k^2}} du^2 \,, \tag{3.2}$$

and the dilaton is given by

$$\phi = \frac{9k}{9k^2-16} \log\left(\sqrt{\frac{C_2}{|C_1|}} \frac{\sinh(\mu_2 |u-u_{02}|)}{\sinh(\mu_1 |u-u_{01}|)} \right) . \tag{3.3}$$

In the vacuum case, due to (3.1) the following relation holds:

$$\frac{\mu_2}{\mu_1} = \frac{4}{3k} > 1 \,. \tag{3.4}$$

From the form of the functions F_1 and F_2 given by (2.48)–(2.49) we can see that the solution will have coordinate singularities at the points u_{01}, u_{02}. We have to consider three coordinate charts. Let us take $\mathbf{u_{02} < u_{01}}$. Then the charts are

3-branch solution

$$\text{left:} \quad u < u_{02} \tag{3.5}$$

$$\text{middle:} \quad u_{02} < u < u_{01} \tag{3.6}$$

$$\text{right:} \quad u > u_{01} \tag{3.7}$$

The degenerate case with $u_{01} = u_{02} = u_0$ requires only two charts:

2-branch solution

$$\text{left:} \quad u < u_0 \tag{3.8}$$

$$\text{right:} \quad u > u_0. \tag{3.9}$$

In figure 2 we plot the solutions for the dilaton ϕ (3.3) for each choice of the coordinates (3.5)–(3.7).

From figure 2 we see that for $u \to u_{01} \pm \epsilon$ the dilaton tends to $-\infty$, while for $u \to u_{02} \pm \epsilon$ the dilaton asymptotes to $+\infty$. It can be verified by direct calculations.

JHEP05(2019)117

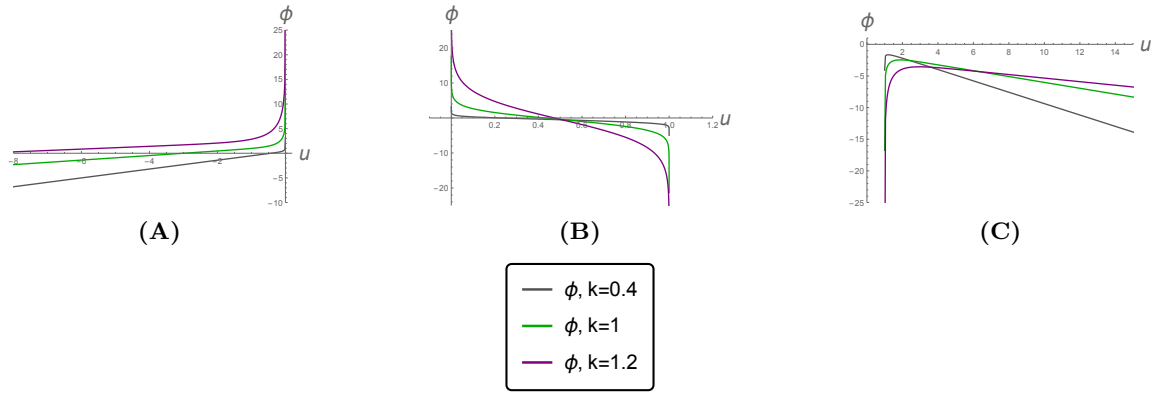

Figure 2. The dilaton solutions (3.3) as functions of u, separately for each type of the solutions: **A)** the dilaton for $u < u_{02}$, $u_{02} = 0$, **B)** the dilaton for $u_{02} < u < u_{01}$, $u_{01} = 1$, $u_{02} = 0$, **C)** the dilaton for $u > u_{01}$, $u_{01} = 1$. For all $E_1 = E_2 = -1$, $C_1 = -C_2 = -1$, $k = 0.4, 1, 1.2$.

3.2 Asymptotics of the metric and the dilaton

We present here the asymptotics of the dilaton (3.3) and the metric (3.2) with (3.5)–(3.7) near the boundaries.

- *The left solution with* $u < u_{02}$
  - at $u \to -\infty$:

$$ds^2 \sim z^{2/3}\left(-dt^2 + dy_1^2 + dy_2^2 + dy_3^2 + dz^2\right), \tag{3.10}$$

$$\phi \sim \frac{9k}{16 - 9k^2}(\mu_2 - \mu_1)\, u \sim \log z \to -\infty, \tag{3.11}$$

    where we use a new coordinate $z \sim \frac{4+3k}{3\mu_1} e^{\frac{3\mu_1 u}{4+3k}}$. In appendix A.2 the scalar curvature of the left solution for both limits is presented. For $u \to -\infty$ the scalar curvature of the left solution (A.19) tends to $+\infty$.
  - at $u \to u_{02} - \epsilon$:

$$ds^2 \sim z^{\frac{18k^2}{64-9k^2}}\left(-dt^2 + dy_1^2 + dy_2^2 + dy_3^2 + dz^2\right), \tag{3.12}$$

$$\phi \sim -\frac{36k}{64 - 9k^2}\log z \to +\infty\,, \tag{3.13}$$

    with the radial coordinate defined by

$$z \sim \frac{64 - 9k^2}{4(16 - 9k^2)}(u - u_{02})^{\frac{64-9k^2}{4(16-9k^2)}}. \tag{3.14}$$

    From the relation for the scalar curvature (A.21) with $u \to u_{02} - \epsilon$ it can be seen that the solution has a non-removable singularity at the point u_{02}.
- *The middle solution with* $u_{02} < u < u_{01}$
  - at $u \to u_{02} + \epsilon$ the asymptotics of the dilaton and the metric are the same as in (3.12)–(3.13). As in the case of the left solution, one can see from the scalar curvature (A.21) that the middle solution has also a singularity at the point u_{02};

JHEP05(2019)117

– at $u \to u_{01} - \epsilon$:

$$ds^2 \sim z^{\frac{8}{9k^2-4}} \left(-dt^2 + dy_1^2 + dy_2^2 + dy_3^2 + dz^2\right), \tag{3.15}$$

$$\phi \sim \frac{9k}{4-9k^2} \log z \to -\infty, \tag{3.16}$$

where the conformal coordinate is

$$z \sim \frac{16-9k^2}{9k^2-4}(u-u_{01})^{\frac{4-9k^2}{16-9k^2}}. \tag{3.17}$$

Notice that as $u \to u_{01}$, the conformal coordinate $z \to 0$ if $0 < k < 2/3$ and $z \to \infty$ if $2/3 < k < 4/3$. These asymptotics are the same as for the solutions in a single exponential potential [9]. It is worth nothing the scalar curvature of the middle solution (A.23) has a regular behaviour at u_{01}.

- *The right solution with* $u > u_{01}$

  – at $u \to u_{01} + \epsilon$ the asymptotics are as in (3.15)–(3.16).

  – at $u \to +\infty$:

$$ds^2 \sim z^{2/3} \left(-dt^2 + dy_1^2 + dy_2^2 + dy_3^2 + dz^2\right), \tag{3.18}$$

$$\phi \sim \log z \to -\infty, \tag{3.19}$$

where z is defined by $z \sim -\frac{4+3k}{3\mu_1} e^{-\frac{3\mu_1 u}{4+3k}}$. The asymptotics are the same as in (3.10)–(3.11). Even though the dilaton goes to $-\infty$, these are different than the asymptotics for a single exponential. The scalar curvature (A.25) goes to $+\infty$ with $u \to +\infty$.

Now let us turn the discussion to the dilaton potential, that can be written on solutions as

$$V = C_1 \left(\frac{F_2}{F_1}\right)^{\frac{18k^2}{9k^2-16}} + C_2 \left(\frac{F_2}{F_1}\right)^{\frac{32}{9k^2-16}}. \tag{3.20}$$

In figure 3 we plot the dilaton potential on the solutions for ϕ. From figure 3C one can see that for the solutions defined for $u > u_{01}$ there is a turning point $V_s = V(\phi)$ with $\phi = \phi_s$, where the potential stops and goes back to zero.

One can find the stop points of the potentials analytically. The stop point u_s can be calculated as follows. The dilaton should obey

$$\phi' = 0, \tag{3.21}$$

this gives rise to

$$\frac{F_1'}{F_1} = \frac{F_2'}{F_2} \tag{3.22}$$

JHEP05(2019)117

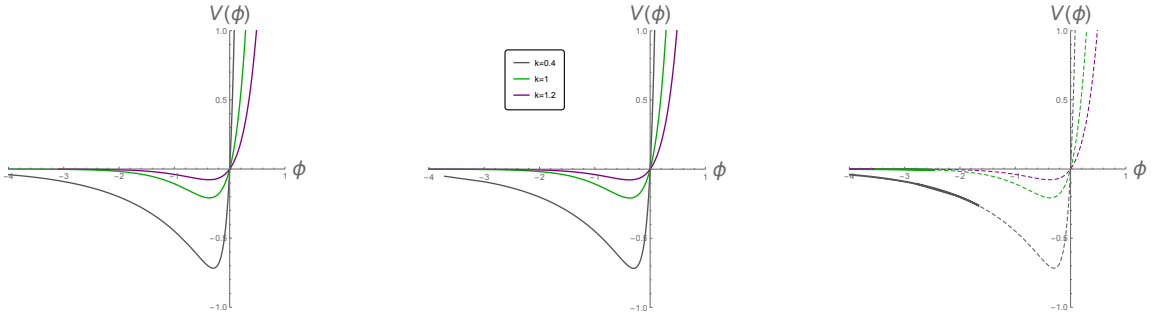

(A) **(B)** **(C)**

Figure 3. The dilaton potential plotted on solutions for ϕ. **A)** The potential in the left-solution varies from $V(\phi_1) = 0$ at $\phi_1 = -\infty$, reaches its minimum and then goes to $V(\phi_2) = +\infty$ at $\phi_2(u_{02} - \epsilon) = +\infty$ (thick lines). **B)** The potential on the middle solution varies from $V(\phi_2) = +\infty$ at $\phi_2 = \phi(u_{02} + \epsilon) = +\infty$ then reaches the minimal value $V_{\min} < 0$ and goes to $V(\phi_1) = 0$ at $\phi_1 = \phi(u_{01} - \epsilon) = -\infty$. **C)** The potential of the right solution varies from $V(\phi_1) = 0$ with $\phi_1 = \phi(u_{01} + \epsilon) = -\infty$ to $V_s < 0$, $V_s = V(\phi)$ at the point $\phi = \phi_s$. When ϕ_s goes back to $-\infty$ the potential goes from $V_s = V(\phi_s)$ back to zero.

and we get

$$\frac{\tanh|\mu_1(u_s - u_{01})|}{\tanh|\mu_2(u_s - u_{02})|} = \frac{\mu_1}{\mu_2}. \tag{3.23}$$

Note, that the value of the potential at the turning point $V_s = V(\phi_s)$ (where $\phi_s = \phi(u_s)$) doesn't coincide with the extremal point of the potential. The extremal point of $V(\phi)$ can also be computed analytically. Using

$$V'_\phi = 2k_1C_1e^{2k_1\phi} + 2k_2C_2e^{2k_2\phi}, \tag{3.24}$$

and taking into account that $C_1C_2 < 0$, we can find

$$\phi_c = \frac{9k}{(16 - 9k^2)}\log\frac{3k}{4} + \frac{9k}{2(16 - 9k^2)}\log\left|\frac{C_1}{C_2}\right|. \tag{3.25}$$

We show the behaviour of the potential as a function of ϕ and the dilaton as a function of u on the same plot in figure 4. In this picture we draw the dependences for all solutions.

3.2.1 Special case $u_{01} = u_{02}$, solutions with AdS boundary

Let us see the features of the solution given by (3.2)–(3.3) with (3.9) and $u_{01} = u_{02} = u_0$.

In figure 5 the behavior of the dilaton (3.3) with $u_{01} = u_{02} = u_0$ is shown. From this picture one can see that the dilaton tends to $-\infty$ as $u \to \pm\infty$.

As for the previous solutions we present the asymptotics in the conformal coordinates.

- In the limit with $u \to \pm\infty$

$$ds^2 \sim z^{2/3}(-dt^2 + dy_1^2 + dy_2^2 + dy_3^2 + dz^2), \tag{3.26}$$

$$\phi \sim \frac{9k}{9k^2 - 16}(\mu_2 - \mu_1)\, u \sim \log z \to -\infty, \tag{3.27}$$

JHEP05(2019)117

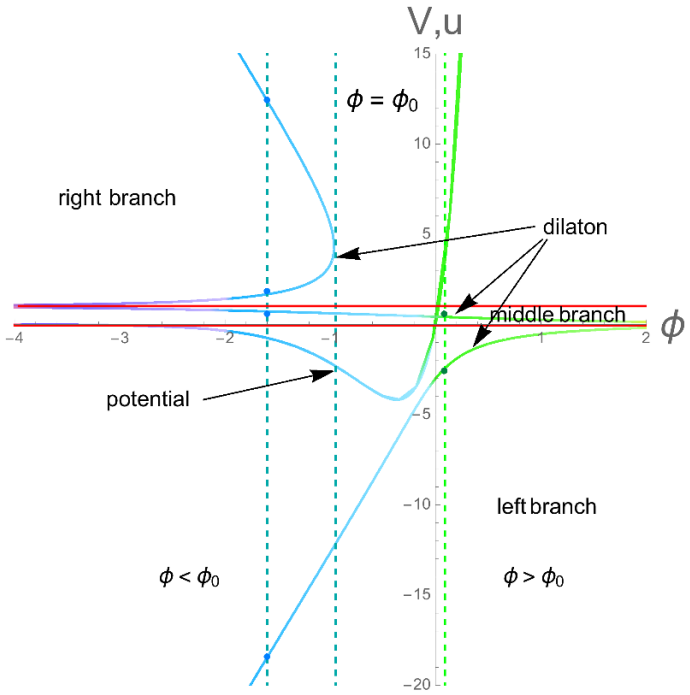

Figure 4. The dilaton potential $V = V(\phi)$ on the vacuum solutions $\phi = \phi(u)$ with (3.5)–(3.7) and plots that indicate which values of u correspond to given ϕ, i.e. $u = u(\phi)$. The function $u(\phi)$ differs for each branch of the solutions, and moreover this function is double-valued at the right branch. The different values of u corresponding to the same ϕ are indicated by points at the vertical lines.

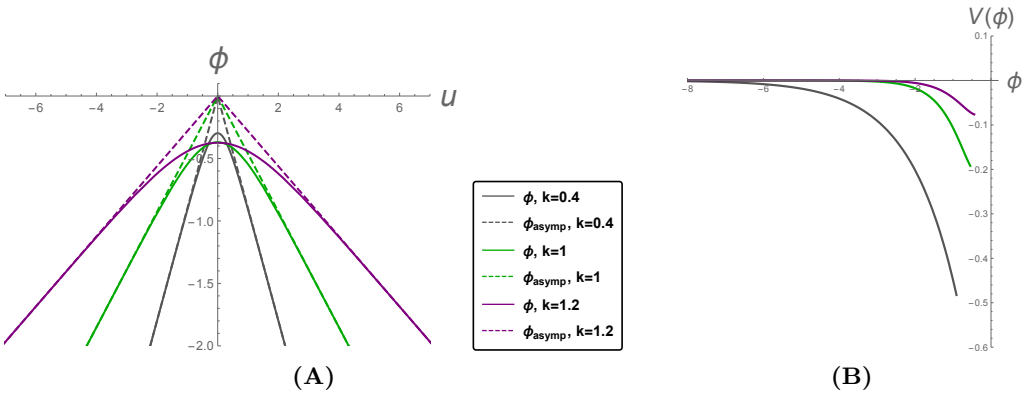

(A) **(B)**

Figure 5. **A)** The behaviour of the dilaton (solid lines) and its asymptotics at infinity (dashed lines) for $u_{01} = u_{02} = 0$, $C_1 = -C_2 = -1$, $E_1 = -E_2 = -1$ and different values of k. From bottom to top $k = 0.4, 1, 1.2$. **B)** The dilaton potential as a function of ϕ for $u > 0$.

JHEP05(2019)117

where the conformal radial coordinate is given by $z \sim \mp\frac{4+3k}{3\mu_1} e^{\mp\frac{3\mu_1 u}{4+3k}}$. So we come to the same asymptotics as for the left (3.10) and right (3.18) solutions with $u \to \pm\infty$ for the 3-branch case. The scalar curvature has also a common behaviour with the right and left solutions, namely it goes to infinity (A.29) with $u \to +\infty$.

- For $u \to u_0$ one gets has the following form of the metric (3.2)

$$ds^2 \sim \frac{1}{z^2}(-dt^2 + dy_1^2 + dy_2^2 + dy_3^2 + dz^2), \tag{3.28}$$

where the conformal "radial" coordinate is defined as $z = 4(u-u_0)^{1/4}$ and $z \to 0$ as $u \to u_0$. In (3.28) one can easily recognize the 5d AdS metric supported by the constant dilaton

$$\phi|_{u\to u_0} \sim \frac{9k}{(16-9k^2)} \log\frac{3k}{4} + \frac{9k}{2(16-9k^2)} \log\left|\frac{C_1}{C_2}\right|, \tag{3.29}$$

which coincides with the minimum of the potential (3.25). As expected the scalar curvature of this solution with $u \to u_0$ has a constant value (A.28).

We note that the figure 5 is an agreement with the calculations of the asymptotics for the dilaton. The potential of the dilaton as a function of ϕ with $u_{01} = u_{02} = u_0$ is presented in figure 5B. From this plot we observe the existence of the turning point of the two-branch solution. The equation for the stop point (3.23) in this case becomes

$$\frac{\tanh(\mu_1 (u_s - u_0))}{\tanh(\mu_2 (u_s - u_0))} = \frac{\mu_1}{\mu_2}, \tag{3.30}$$

and has a solution

$$u_s = u_0. \tag{3.31}$$

As already observed, in this case we find that the stop point coincides with the extremal point of the potential, $\phi_s = \phi_c = \phi(u_0)$.

3.3 RG flow for vacuum solutions

3.3.1 Details of RG flow for vacuum solutions

The domain wall form (2.57) of the vacuum solutions looks

$$ds^2 = e^{2\mathcal{A}}\Big[-dt^2 + dy_1^2 + dy_2^2 + dy_3^2\Big] + dw^2. \tag{3.32}$$

To come to (3.32) we use the change of variables for (3.2)–(3.3)

$$dw = F_1^{\frac{16}{9k^2-16}} F_2^{\frac{9k^2}{16-9k^2}}\, du. \tag{3.33}$$

We can represent the scale factor of the domain wall (3.32) as follows

$$\mathcal{A} = \frac{4}{9k^2-16} \log F_1 + \frac{9k^2}{4(16-9k^2)} \log F_2, \tag{3.34}$$

JHEP05(2019)117

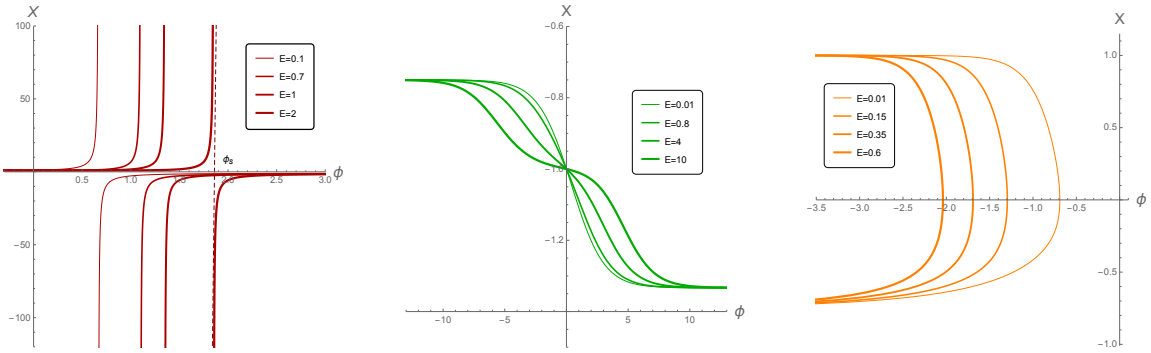

(A) **(B)** **(C)**

Figure 6. The behaviour of the X-function with the dependence on the dilaton plotted using the solutions for $\mathcal{A}$ and ϕ: **A)** the left branch with $u_{02} > u$, **B)** the middle branch $u_{02} < u < u_{01}$; **C)** the right branch $u > u_{01}$. For all plots $u_{01} = 0$, $u_{02} = -1$, $k = 1$, $C_1 = -2$, $C_2 = 2$, different curves on the same plot correspond to the different values of $|E_1| = |E_2|$, labeled as E on the legends.

so the energy scale A is

$$\mathrm{A} \equiv e^{\mathcal{A}} = F_1^{\frac{4}{9k^2-16}} F_2^{\frac{9k^2}{4(16-9k^2)}}. \tag{3.35}$$

The running coupling is defined through the dilaton (3.3) reads

$$\lambda = \left(\frac{F_2}{F_1}\right)^{\frac{9k}{9k^2-16}}. \tag{3.36}$$

The function X (2.59) is represented as follows

$$X = \frac{1}{3}\left(\frac{F_2}{F_1}\right)^{\frac{9k}{16-9k^2}} \frac{\lambda'}{\mathcal{A}'}, \tag{3.37}$$

with λ given by (3.36), $\mathcal{A}$ — by (3.34). It is useful to explore the evolution of the rescaled β-function X (3.37) as a function of log of the running coupling (3.36), which is the dilaton ϕ. In figure 6 we present the parametric plots of the behaviour of X (3.37) using solutions for ϕ (2.46) and $\mathcal{A}$ (3.34) with the dependence on the parameter u (3.5)–(3.7). In these plots we fix the shape of the potential putting $C_1 = -C_2 = -2$ and $k = 1$ while we vary the constants $|E_1| = |E_2|$ (labeled as E in figure 6). From picture 6A and 6C we see that the holographic β-functions at zero temperature constructed on the left $u < u_{02}$ and right solutions $u > u_{01}$ can take both negative and positive values. As for the case 6B, which corresponds to the middle solution, X is always negative.

It is also of our interest to see the function $X(\phi)$ plotted on the solutions with $u_{01} = u_{02} = u_0$, particularly for $u_0 = 0$. In figure 7 we show the function $X(\phi)$ on the dilaton solution (3.3) with $u_{01} = u_{02}$. We see that the behaviour of the function $X(\phi)$ is the same for all values of E_2. From figures 6–7 we see that X are regular except those plotted on the left solutions on figure 6A at some points ϕ_s where $X(\phi_s)$ takes an infinite value. From

JHEP05(2019)117

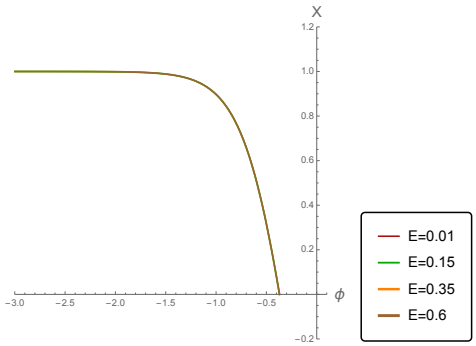

Figure 7. The $X(\phi)$ function for the dilaton solution with $u_{01} = u_{02} = 0$, the potential fixed as $C_1 = -2$, $C_2 = 2$, $k = 1$. For all range of values of $|E_1| = |E_2|$, labeled as E on the legend, the curves of X coincide.

eq. (3.37) with $\alpha^1 = 0$ one can see that X is infinite with $\mathcal{A}' = 0$, i.e.

$$9k^2\frac{F_2'}{F_2} - 16\frac{F_1'}{F_1} = 0. \tag{3.38}$$

Eq. (3.38) defines the singular point u_s, which is related to ϕ_s. The singular point ϕ_s coincides with the point where $\mathcal{A}' = 0$, and its position depends on E, k, u_{01} and u_{02}, see figure 8A. From this picture we see that for the left solution the dilaton varies from $-\infty$ to a special value ϕ_s, the scale factor is non-monotonic function increases, but after the dilaton passes this special value ϕ_s, the scale factor starts to decrease. From figure 8B we observe that the scale factor $\mathcal{A}$ has a monotonic behaviour, decreasing with respect to dilaton running from $-\infty$ to $+\infty$. Figure 8C it is demonstrated by orange curves that the scale factor of the right solution decreases from $+\infty$ to $-\infty$ for all values of the dilaton, which runs from $-\infty$ to some constant value and then goes back to $-\infty$. We also present that the behavior of the scale factor $\mathcal{A}$ on ϕ for the solution with $u_{01} = u_{02} = 0$ by the brown curve in figure 8C. We see that the scale factor for this solution starts to decrease from $+\infty$ with some constant value of the dilaton, then, passing some value of $\mathcal{A}$, both the scale factor and the dilaton tend to $-\infty$.

In the section 2.5 it was already said that the system (2.61)–(2.62) on the vacuum solutions reduces to eq. (2.63), which is quite simple and one can treat it in the general form. We remind that the dilaton potential is given by (2.2) and in the cases presented at the plots below

$$V = -2e^{2k\phi} + 2e^{\frac{32}{9k}\phi}, \tag{3.39}$$

with $k = k_1$ and $k_2 = \frac{16}{9k_1}$ (a constraint from the solution) and $C_1 = -2$, $C_2 = 2$. The values of the dilaton coupling constant have the following restriction $0 < k < 4/3$.

Taking into account (3.39) we have

$$\frac{d\log V}{d\phi} = \frac{-2ke^{2k\phi} + \frac{32}{9k}e^{\frac{32}{9k}\phi}}{-e^{2k\phi} + e^{\frac{32}{9k}\phi}}. \tag{3.40}$$

The solution to (2.63) with (3.39)–(3.40) is represented in figure 9 using StreamPlot. On this figure we observe all possible solutions for X (blue curves) to our model with the

JHEP05(2019)117

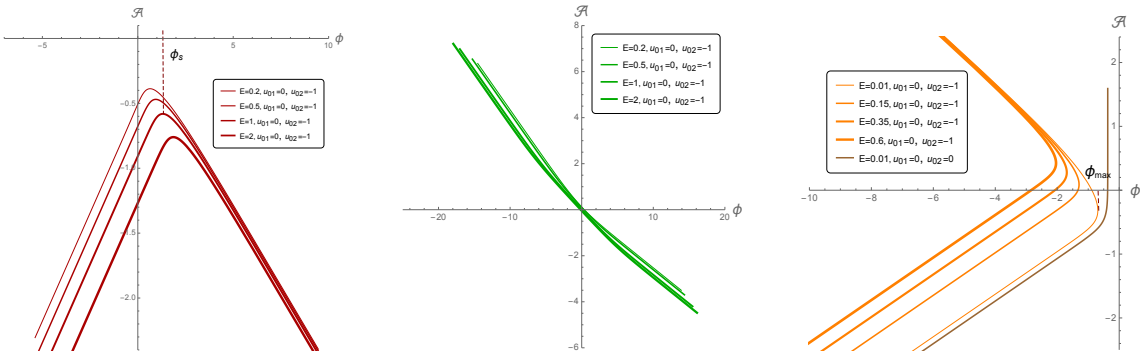

Figure 8. The behaviour of $\mathcal{A}$ as a function of ϕ for the vacuum solutions, we fix values of $u_{01} = 0$ and $u_{02} = -1$ and varying $|E_1| = |E_2|$, denoted as E: **A)** the left solutions, **B)** the middle solutions, **C)** the right solutions by orange curves; the solution with $u_{01} = u_{02}$ and $E = 0.01$ by the brown curve.

potential (3.39). We also impose figures 6 and 7 on figure 9A and see that they can partially cover the plot. In figure 9A the red lines correspond to the left solution, see figure 6A, the green lines are those from the middle solution, see figure 6B, the orange ones correspond to the right solution, see figure 6C. In figure 9A we observe that the function X corresponding to the right solution (the orange curves) interpolates between X_{c2} and 1. The X for the middle solution (the green curves) interpolates between X_{c1} and X_{c2} in figure 9. The dark red curves start at 1 and go to $+\infty$ as $\phi \to \phi_s - 0$, some of these lines have local minimum and are located very close to the brown curve corresponding to the vacuum flow for the two branch solution $u_{01} = u_{02}$. The flow with local maximum in figure 9A corresponds to our solutions with small difference between u_{01} and u_{02}. The darker red lines in the right bottom part of 9A start at X_{c1} and go to $-\infty$ when $\phi \to \phi_s + 0$. For the fixed form of the potential the point ϕ_s is defined by values of $|E_1| = |E_2| = E$, u_{01}, u_{02}, i.e. $\phi_s = \phi_s(E, u_{01}, u_{02})$.

We see that in figure 9A some parts of the RG flow (the stream at the left bottom part as well as the stream at the right upper part that interpolates between -1 and 1) are not covered by our vacuum solutions (2.48), (2.49). However, it was already pointed in section 2.3 that analytic solutions for $\mathcal{A}$ and ϕ can be governed by F_1 and F_2 that are sin- or linear functions, namely (2.52)–(2.53) and (2.54). Since the equation (2.63) doesn't know about our choice of the solutions and we see on the plot all possible solutions, and the curves of the dependence $X(\phi)$ on ϕ built on (2.52)–(2.54) should appear on the plot. In figure 9B we present the stream of (2.63) by blue lines, $X(\phi)$ on ϕ plotted using (2.52)–(2.53) by grey lines and $X(\phi)$ related to (2.54) by the dark red dashed lines, correspondingly. We see that these lines partially fit the solutions to equation (2.63). We show separately the behaviour of $X(\phi)$ with (2.54) in figure 9C. From figures 9A and 9B we see that $X(\phi)$ corresponding to the linear solutions can be considered as a boundary between $X(\phi)$ corresponding to "sin"-solutions and $X(\phi)$ goverened by the left sinh-solutions (i.e. sinh-solutions with $u < u_{02}$).

However, we still observe in figures 9B and 9C that some regions of the figure are not covered. If we look at the equation (2.63) it is evidently that it is invariant under the

JHEP05(2019)117

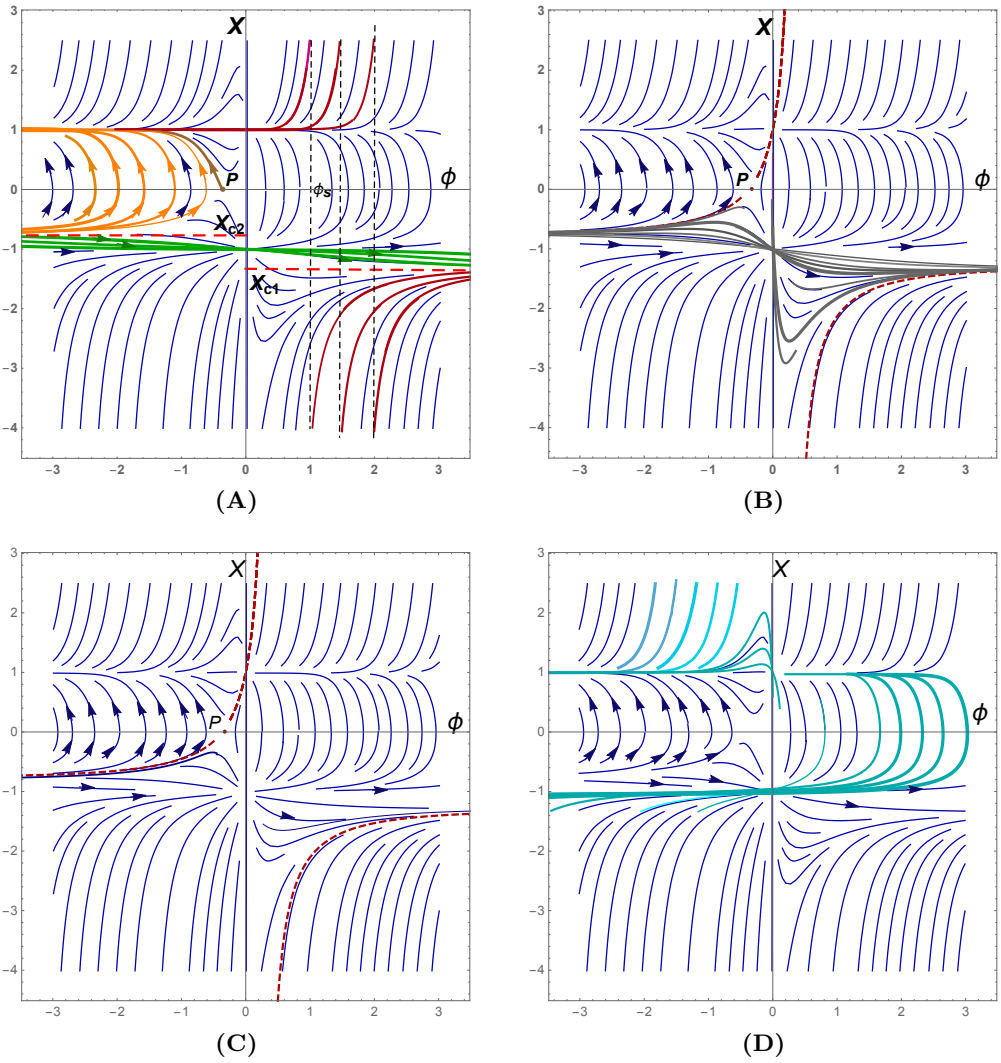

Figure 9. The plots show how the solutions X to (2.63) obtained numerically as stream plots can be recovered by the explicit solutions given by eqs. (2.48), (2.49), (2.52), (2.53) and (2.55). In all plots, the blue lines represent the stream lines of the solutions of (2.63) for $C_1 = -C_2 = -2$ and $k = 1$. The explicit solutions are represented by the colored lines. **A)** The orange, green and dark red curves show $X = X(\phi)$ on the right, middle and the left solutions, respectively, of (2.48), (2.49). We see that solutions on left solutions have jumps at some values of u indicated by the black dashed lines. **B)** The grey curves show $X = X(\phi)$ built on the analytic solutions with sin-formula (2.52)–(2.53), the red dashed lines show $X = X(\phi)$, given by the "linear"-formula (2.54). **C)** Separately, the dark red dashed lines show $X = X(\phi)$ governed by "linear"-functions (2.54). **D)** The cyan lines present the behaviour of $X(\phi)$ governed by cosh-functions (2.55)–(2.56). For all plots different thickness of curves corresponds to different values of $|E_1| = |E_2|$.

JHEP05(2019)117

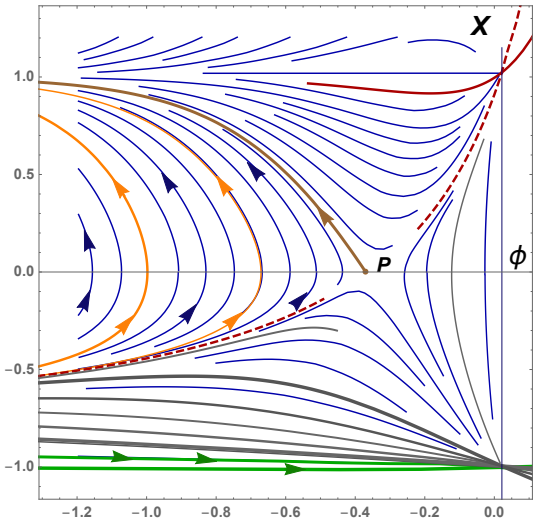

Figure 10. The behaviour of $X(\phi)$ near the point P plotted using exact vacuum solutions and the stream of eq. (2.63) (blue lines). The legends are the same as in figure 9.

change of the sign of the potential (3.39), i.e. $V \to -V$. So the stream of eq. (2.63) should include also solutions to equations of motions with $-V$. In section 2.3 we see that, indeed, these are solutions with F_1 and F_2 governed by cosh-functions (2.55)–(2.56).

In figure 9D we draw $X(\phi)$ as a solution to (2.63) (blue lines) and with the help of the analytical solution related to (2.55)–(2.56) (the curves of other colors), that perfectly complete the necessary part of the stream.

Let's look at figures 9A and 9B more closely. On these pictures we see a special point P, which is a stationary point of our potential $V'(\phi) = 0$. We zoom the scale near the point P in figure 10 to see the behaviour of the vacuum $X(\phi)$ functions near P in details. As in the previous figures we show the stream of eq. (2.63) by blue curves and by the other color curves the functions $X(\phi)$ plotted using analytic solutions for $\mathcal{A}$ and ϕ.

It worth to be noted that in figures 9 and 10 the arrows always show the direction of decreasing scale factor $\mathcal{A}$, see figure 8, that corresponds to the flow from UV fixed point to IR.

3.3.2 The running coupling $\lambda = e^{\phi}$ on the energy scale

It is important to know the behaviour of the running coupling $\lambda = e^{\phi}$ on the energy scale $\mathrm{A} = \exp \mathcal{A}$. One can trace this using the analytic solutions for ϕ and $\mathcal{A}$. For the vacuum case both of them depend on the constant of integration E_1, E_2, u_{01}, u_{02} and on the shape of the potential, which is defined by C_1, C_2 and k.

Let us see how the energy scale A depends on u. In in figure 11A we observe that A is non-monotonic function for the left solutions. First it increases, but near u_{02} it decreases that can be clearly seen in the zoomed picture figure 11B. This non-monotonic behaviour is also read from figure 8 for the behaviour of the energy A on the dilaton for the left branch.

In figure 12 the dependence of the coupling constant $\lambda = \exp \phi$ on the scale A is presented for the zero-temperature solutions with (3.5)–(3.7) and figure 12C with (3.9).

JHEP05(2019)117

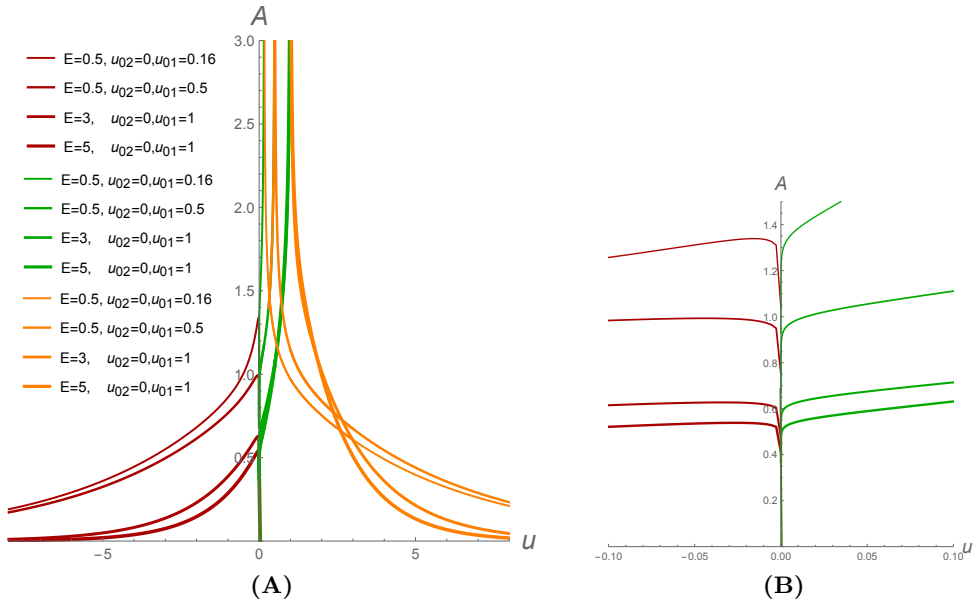

(A) **(B)**

Figure 11. The behaviour of the energy scale A at all 3 branches (the darker red curves for the left solution, the green ones for the middle and the orange ones for the right solution) and its zoom near $u_{02} = 0$. For all plots $k = 1$, $C_1 = -2$, $C_2 = 2$, different curves on the same plot correspond to the different values of $|E_1| = |E_2|$, labeled as E, different u_{01} and u_{02}.

We recall that on the left and middle solutions the dilaton interpolates between $\pm\infty$ and for the right solution it starts at $-\infty$ goes to the maximal value $\phi_{\max}$ and then goes back to $-\infty$ (we have observed this behaviour already in the previous sections). In spite of that the dilaton has the similar behaviour on the left and middle solutions, the scale factor has rather different behaviour on these solutions, namely, on the middle solution the scale factor monotonically decreases from large positive values to zero as the dilaton runs from $+\infty$ to $-\infty$. The right solution is a bouncing solution with the decreasing scale factor. These behaviours of the scale factors and the dilaton are reflected in the plots for the dependence of the running coupling on the energy scale.

We can summarize the results for the running coupling in the following form

- as expected for solutions with $u < u_{02}$, see figure 12A, where the dilaton tends to $-\infty$ in the IR region and we have IR-free theory, while in the UV region the effective coupling $\lambda \to +\infty$.

- In figure 12B we see that the dependence of λ on A plotted on the middle solutions with $u_{02} < u < u_{01}$ mimics the QCD behavior.

- The running coupling plotted as a function of the energy scale at figure 12C for the solutions with (3.7) shows that it is UV free as well as IR free theory, i.e. the running coupling has the form of the hill.

JHEP05(2019)117

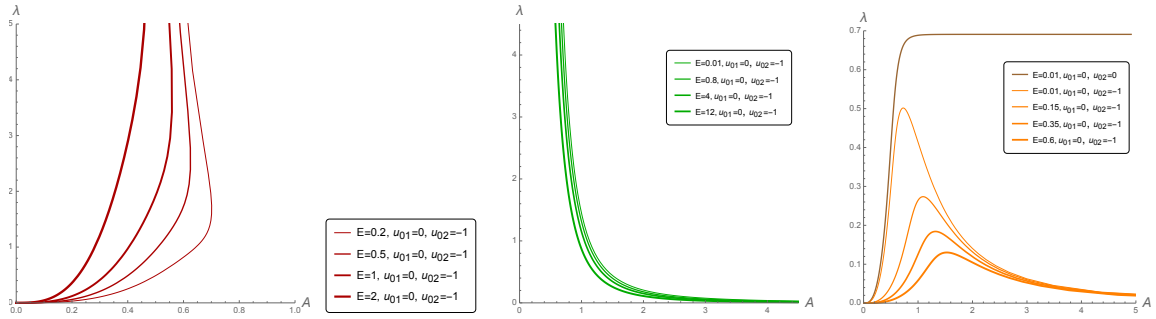

(A) **(B)** **(C)**

Figure 12. The dependence of the coupling constant on the energy A on the dilaton plotted using the solutions for $\mathcal{A}$ and ϕ: **A)** the left branch with $u_{02} > u$, **B)** the middle branch $u_{02} < u < u_{01}$; **C)** the right branch $u > u_{01}$. For all plots $k = 1$, $C_1 = -2$, $C_2 = 2$, different curves on the same plot corresponds to the different values of $|E_1| = |E_2|$, labeled as E on the legends and different u_{01} and u_{01} also indicated on the legends.

4 Non-vacuum solutions

4.1 The metric and the dilaton

The metric and the dilaton solutions to the model (2.1) in the non-vacuum case are

$$ds^2 = F_1^{\frac{8}{9k^2-16}} F_2^{\frac{9k^2}{2(16-9k^2)}} \left(-e^{2\alpha^1 u} dt^2 + e^{-\frac{2\alpha^1}{3}u} d\vec{y}^2\right) + F_1^{\frac{32}{9k^2-16}} F_2^{\frac{18k^2}{16-9k^2}} du^2, \tag{4.1}$$

$$\phi = -\frac{9k}{9k^2-16} \log F_1 + \frac{9k}{9k^2-16} \log F_2, \tag{4.2}$$

where the functions F_1 and F_2 are given by (2.48)–(2.49) as before.

Just as in the vacuum case, we need to separate the solutions in the branches (3.5)–(3.9) with respect to values of u_{01} and u_{02}. We note that the factors of α^1 in the metric (4.1) break the Poincaré symmetry. However, below we will see that the presence of this parameter allows us to define a horizon and to construct black branes. We also recall that E_1 and E_2 must obey the constraint

$$E_1 + E_2 + \frac{2}{3}(\alpha^1)^2 = 0. \tag{4.3}$$

The condition (4.3) allows to tune parameters thus we have two additional regimes

$$1)\ \mu_1 = \mu_2, \quad 2)\ \mu_1 > \mu_2, \tag{4.4}$$

with

$$1)\ E_2 = \frac{6k^2(\alpha^1)^2}{16-9k^2}, \quad 2)\ E_2 < \frac{6k^2(\alpha^1)^2}{16-9k^2}, \tag{4.5}$$

respectively.

This leads to new dynamics of the dilaton (4.2). Particularly, the dilaton can be constant, that is inapplicable for the vacuum case where it always holds $\mu_2 = \frac{4}{3k}\mu_1$.

JHEP05(2019)117

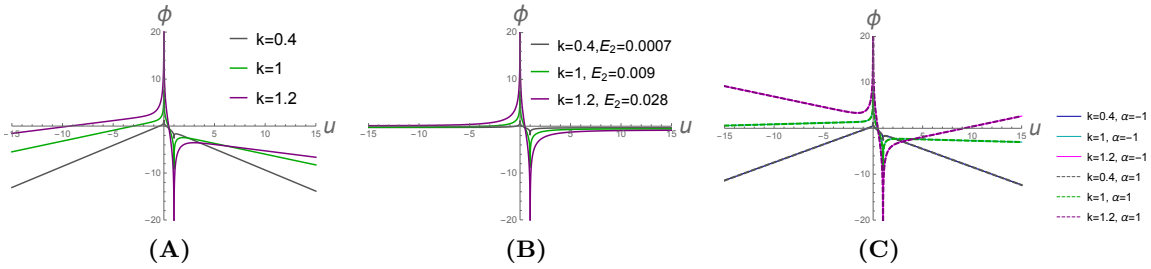

Figure 13. The dilaton for the 3-branch solutions with $u_{01} = 1, u_{02} = 0$ and $C_1 = -1$, $C_2 = 1$ in the non-vacuum case: **A)** $\alpha^1 = -0.1$, $E_2 = 1$, and different k; **B)** $E_2 = 0.0007$ for $k = 0.4$, $E_2 = 0.009$ for $k = 1$, $E_2 = 0.028$ for $k = 1.2$; $\alpha^1 = -0.1$ for all; **C)** solid lines correspond to $\alpha^1 = -1$ and dashed lines to $\alpha^1 = 1$, $k = 0.4, 1, 1.2$, $E_2 = 1$ for all. The dashed and solid lines coincide.

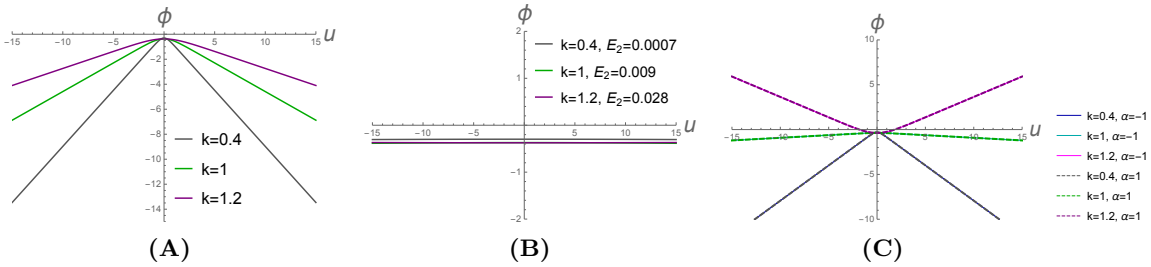

Figure 14. The dilaton for the 2-branch solutions $C_1 = -1$, $C_2 = 1$ and $u_{01} = u_{02} = 0$ in the non-vacuum case: **A)** $\alpha^1 = -0.1$, $E_2 = 1$ and different k, **B)** $E_2 = 0.0007$ for $k = 0.4$, $E_2 = 0.009$ for $k = 1$, $E_2 = 0.028$ for $k = 1.2$; $\alpha^1 = -0.1$ for all; **C)** solid lines correspond to $\alpha^1 = -1$ and dashed lines to $\alpha^1 = 1$, $k = 0.4, 1, 1.2$, $E_2 = 1$ for all. The dashed and solid lines coincide.

We illustrate the behaviour of the dilaton solution for the non-vacuum case in figure 13 for branches (3.5)–(3.7) with $u_{01} \neq u_{02}$. As it was expected the condition (4.3) changes the behaviour of the dilaton. In figure 13B we plot the dilaton keeping the same shape of the potential and the value of α^1 as for figure 13A, but the values of the parameter E_2 are changed with respect to (4.5). In figure 13C we again save the form of the potential, use the same value of E_2 as in 13A, take bigger α^1 and show that the opposite sign of this parameter doesn't change the asymptotics of the dilaton. From figure 13C one observes that for $u \to \pm\infty$ ϕ can tend to $+\infty$, while for the vacuum case $\phi \to -\infty$ as $u \to \pm\infty$. In figure 13C we also see the behaviour of the dilaton doesn't depend on the sign of the parameter α.

In figure 14 we plot the dependences of the dilaton solution with $u_{01} = u_{02} = u_0$ on u (3.9). As for the 3-branch solutions from figure 14B we see that the dilaton can be constant with the appropriate choice of parameters agreed with (4.3) and can change its asymptotics from $-\infty$ to $+\infty$ at $u \to \pm\infty$, see figure 14C.

In figure 15 we draw the potential V as a function of ϕ and the dependence u on ϕ. The functions $u(\phi)$ are different on the different branches. The different values of u corresponding to the same ϕ are indicated by points at the vertical lines. We see that

JHEP05(2019)117

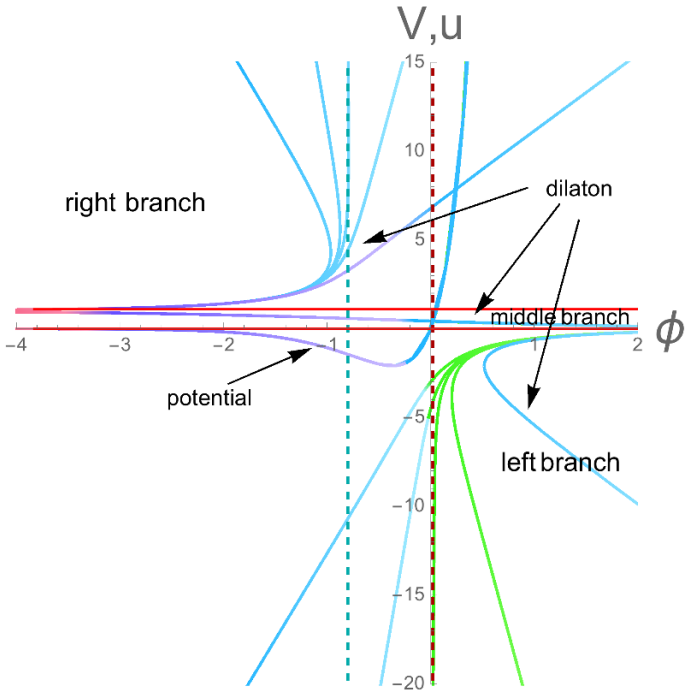

Figure 15. The dilaton potential $V = V(\phi)$ on non-vacuum solutions $\phi = \phi(u)$ with (3.5)–(3.7) and plots that indicate which values of u correspond to given ϕ, i.e. $u = u(\phi)$.

the function $u(\phi)$ for $|\alpha^1| < \alpha^1_{cr}$ is double-valued on the right branch, and for $|\alpha^1| > \alpha^1_{cr}$ it is double-valued on the left branch, and for $|\alpha^1| = \alpha^1_{cr}$ the both functions one-to-one functions for all branches, and $\phi < \phi_0'$ for the right branch and $\phi > \phi_0''$ at the left branch.

The dilaton potential which is plotted in figure 15 on the right solutions for the dilaton is bounded above like for the vacuum right solutions.

4.2 The black brane solutions

Now we are going to find a black brane representation of the solution (4.1)–(4.2) defined for (3.7) with $u_{01} \neq u_{02}$. The metric (4.1) can be rewritten in the following form

$$ds^2 = \mathcal{C}\,\mathcal{X}(u) e^{\kappa u - \frac{2}{3}\alpha^1 u} \left(-e^{\frac{8}{3}\alpha^1 u} dt^2 + d\vec{y}^2 + \mathcal{X}(u)^3 \mathcal{C}^3 e^{\left(3\kappa + \frac{2}{3}\alpha^1\right)u} du^2 \right), \tag{4.6}$$

with the constant $\mathcal{C}$ given by

$$\mathcal{C} \equiv \left(\frac{1}{2}\sqrt{\left|\frac{C_1}{2E_1}\right|} e^{-\mu_1 u_{01}} \right)^{\frac{8}{9k^2-16}} \left(\frac{1}{2}\sqrt{\left|\frac{C_2}{2E_2}\right|} e^{-\mu_2 u_{02}} \right)^{\frac{9k^2}{2(16-9k^2)}}, \tag{4.7}$$

the function $\mathcal{X}(u)$ written as

$$\mathcal{X}(u) = \left(1 - e^{-2\mu_1 (u-u_{01})}\right)^{-\frac{8}{16-9k^2}} \left(1 - e^{-2\mu_2 (u-u_{02})}\right)^{\frac{9k^2}{2(16-9k^2)}} \tag{4.8}$$

and the exponent κ given by

$$\kappa \equiv \frac{8}{\sqrt{6\,(16-9k^2)}} \left(-\sqrt{E_2 + \frac{2}{3}(\alpha^1)^2} + \frac{3}{4} k \sqrt{E_2} \right), \tag{4.9}$$

JHEP05(2019)117

where we took into account the relations for μ_1 and μ_2 (2.48)–(2.49). We see that for $0 < k < 4/3$ one has $\kappa < 0$.

To have the black brane solutions we need to remove a conical singularity in the metric (4.6) (since with $\alpha^1 < 0$ we get zero in front of dt^2). Taking

$$e^{\frac{4}{3}\alpha^1 u} = \rho, \quad t = i\tau, \tag{4.10}$$

so the metric reads

$$ds^2 \underset{u\to\infty}{\sim} \frac{\mathcal{C}^4}{\left(\frac{4}{3}\alpha^1\right)^2}\mathcal{X}e^{\kappa u-\frac{2}{3}\alpha^1 u}\left(\frac{1}{\mathcal{C}^3}\left(\frac{4}{3}\alpha^1\right)^2\rho^2 d\tau^2+\frac{1}{\mathcal{C}^3}\left(\frac{4}{3}\alpha^1\right)^2 d\bar{y}^2+\mathcal{X}^3 e^{3(\kappa-\frac{2}{3}\alpha^1)u}d\rho^2\right), \tag{4.11}$$

where $\mathcal{X}(u) \to 1$ for $\rho \to 0$ as $u \to \infty$.

Therefore, there is no conic singularity if the following constraint is satisfied

$$\kappa - \frac{2}{3}\alpha^1 = 0. \tag{4.12}$$

We also fix the periodicity

$$\frac{4}{3\mathcal{C}^{3/2}}\alpha^1\beta = 2\pi. \tag{4.13}$$

Plugging (4.9) in (4.12) we come to the condition to the parameters

$$E_1 = -\frac{32(\alpha^1)^2}{3(16-9k^2)}, \quad E_2 = \frac{6k^2(\alpha^1)^2}{16-9k^2}, \tag{4.14}$$

that corresponds to $\mu_1 = \mu_2 = \mu$ with

$$\mu = -\frac{4}{3}\alpha^1. \tag{4.15}$$

Therefore, we get the black brane, if (4.12) is satisfied, and the temperature is

$$\frac{1}{\beta} = T = \frac{2}{3\pi}\frac{|\alpha^1|}{\mathcal{C}^{3/2}}. \tag{4.16}$$

Here $\mathcal{C}$ is taken with the constraint (4.15), see (4.19) below.

Under the condition (4.12) the black brane metric has the form

$$ds^2 = \mathcal{C}\,\mathcal{X}\Big(-e^{-2\mu u}dt^2 + d\bar{y}^2\Big) + \mathcal{C}^4\,\mathcal{X}^4 e^{-2\mu u}du^2, \tag{4.17}$$

where $\mathcal{C}$ and $\mathcal{X}$ are given by

$$\mathcal{X} = (1-e^{-2\mu u})^{-\frac{8}{16-9k^2}}(1-e^{-2\mu(u-u_{02})})^{\frac{9k^2}{2(16-9k^2)}}, \tag{4.18}$$

$$\mathcal{C} \equiv 2^{\frac{16}{(16-9k^2)}}(3\mu)^{\frac{1}{2}}|C_1|^{\frac{8}{2(9k^2-16)}}\left(\frac{C_2}{k}e^{-2\mu u_{02}}\right)^{\frac{9k^2}{4(16-9k^2)}}(16-9k^2)^{-\frac{1}{4}} \tag{4.19}$$

JHEP05(2019)117

with the horizon located at $u = +\infty$ and the near-horizon expansion of $\mathcal{X}(u)$ is

$$\mathcal{X} \approx 1 + e^{-2\mu u}\left(\frac{16 - 9k^2 e^{2\mu u_{02}}}{2(16-9k^2)}\right). \tag{4.20}$$

We note that the boundary is at u_{01} and we fixed $u_{01} = 0$ to have $f = 1$ at this boundary. One can check that null geodesics we have the correct behaviour. Null geodesics imply

$$ds^2 = 0, \tag{4.21}$$

i.e. for the light moving in the radial direction

$$\frac{dt}{du} = \pm e^{3A+\frac{3}{4}\mu}, \tag{4.22}$$

or

$$\begin{aligned} t - t_0 &\sim \int_{u_0}^{u} d\bar{u} e^{\left(\frac{3}{2}\kappa + \frac{3\mu}{4}\right)\bar{u}} \mathcal{C}^{3/2}\left(1 + \frac{3\left(16 - 9k^2 e^{2\mu u_{02}}\right)}{4(16-9k^2)} e^{-2\mu\bar{u}}\right) \\ &= \int_{u_0}^{u} d\bar{u}\mathcal{C}^{3/2}\,(1+\ldots) \underset{u\to\infty}{\to} \infty. \end{aligned} \tag{4.23}$$

This calculation confirms that we have the horizon at $u = +\infty$.

The scalar curvature and the Kretschmann scalar near horizon $u \to +\infty$ are

$$R = \left(\frac{C_1}{2E_1}\right)^{\frac{16}{16-9k^2}} \left(\frac{C_2}{2E_2}\right)^{-\frac{9k^2}{16-9k^2}} \left(\frac{3(16\mu_1 - 9k^2\mu_2)^2}{4(16-9k^2)^2} - \frac{4}{3}\left(\alpha^1\right)^2\right) e^{\frac{2(16\mu_1 - 9k^2\mu_2)}{16-9k^2}u}, \tag{4.24}$$

$$\begin{aligned} K = &\frac{\left(4\alpha^1(9k^2-16) + 27k^2\mu_2 - 48\mu_1\right)^2}{864(16-9k^2)^4} \left(\frac{C_1}{2E_1}\right)^{\frac{32}{16-9k^2}} \left(\frac{C_2}{2E_2}\right)^{\frac{18k^2}{9k^2-16}} e^{\frac{4(16\mu_1 - 9k^2\mu_2)}{16-9k^2}u} \\ &\cdot \left(304(\alpha^1)^2(16-9k^2)^2 + 168\alpha^1(9k^2-16)(16\mu_1 - 9k^2\mu_2) + 63(16\mu_1 - 9k^2\mu_2)^2\right). \end{aligned} \tag{4.25}$$

We note that with respect to the constraint to absence of the conic singularity (4.11) both the scalar curvature (4.24) and Kretschmann scalar (4.25) tend to zero with $u \to +\infty$.

4.2.1 The Gubser bound

The dilaton supporting the geometry (4.17) reads

$$\phi = \frac{9k}{9k^2-16}\log\left[\frac{4}{3k}\sqrt{\left|\frac{C_2}{C_1}\right|}\frac{\sinh(\mu(u-u_{02}))}{\sinh(\mu u)}\right] \tag{4.26}$$

and takes the constant value near horizon

$$\lim_{u\to+\infty}\phi = \frac{9k}{9k^2-16}\left(\log\left(\frac{4}{3k}\sqrt{\left|\frac{C_2}{C_1}\right|}\right) - \mu u_{02}\right). \tag{4.27}$$

Now one can check if the Gubser's bound [22] for asymptotically non-AdS solutions holds

$$V(\phi(u_h)) < 0, \tag{4.28}$$

JHEP05(2019)117

where in our case $u_h = \infty$. Plugging the solutions for the dilaton at the horizon (4.27) in (2.2) the inequality (4.28) takes the form

$$\frac{E_2}{|E_1|} - 1 < 0, \tag{4.29}$$

that is valid for our solution due to the constraint (4.3). The improved Gubser's bound (4.28) reads

$$V(\phi(u_h)) \leq V_{\rm UV}, \tag{4.30}$$

where $V_{\rm UV}$ is the value of $V(\phi)$ at ultraviolet fixed point. Since $V_{\rm UV} = 0$ with the dilaton $\phi \to -\infty$ at the UV point the constraint (4.30) comes to be (4.28).

In the UV limit, i.e. near $u_{01} = 0$, the solutions turns to have the asymptotics as the Chamblin-Reall solution governed by the single exponential potential

$$ds^2 \sim z^{\frac{8}{9k^2-4}} \left(-dt^2 + d\vec{y}^2 + dz^2\right), \tag{4.31}$$

with the dilaton

$$\lim \phi_{u\to u_{01}+\epsilon} = -\frac{9k}{16-9k^2} \log\left[\frac{4}{3k}\sqrt{\frac{C_2}{|C_1|}}\frac{\sinh(-\mu\, u_{02})}{\mu\,\epsilon}\right]. \tag{4.32}$$

We note that we can construct a black brane background for the left solutions (3.5) with $u_{01} \neq u_{02}$ assuming that the horizon is located at $u = -\infty$, and the parameter α^1 is positive.

4.2.2 Special case $u_{01} = u_{02}$, AdS black brane

Now we turn to the special case of the non-vacuum solutions with $u_{01} = u_{02} = 0$ with $u > 0$. The construction of a black brane metric is the same as presented before for solutions with $u_{01} \neq u_{02}$ with the horizon located at $u = +\infty$. The metric (4.17) has the form

$$ds^2 = \mathcal{C}\left(1 - e^{-2\mu u}\right)^{-\frac{1}{2}} \left(-e^{-2\mu u}dt^2 + d\vec{y}^2\right) + \mathcal{C}^4 \left(1 - e^{-2\mu u}\right)^{-2} e^{-2\mu u} du^2, \tag{4.33}$$

where we took into account $\mu = -\frac{4}{3}\alpha^1$ and the constant $\mathcal{C}$ reads

$$\mathcal{C} \equiv 2^{\frac{16}{(16-9k^2)}} (3\mu)^{\frac{1}{2}} \Big(|C_1|\Big)^{\frac{8}{2(9k^2-16)}} \left(\frac{C_2}{k}\right)^{\frac{9k^2}{4(16-9k^2)}} (16-9k^2)^{-\frac{1}{4}}. \tag{4.34}$$

Due to the constraint $\mu_1 = \mu_2$ and $u_{01} = u_{02}$ the dilaton (4.2) becomes constant

$$\phi = \frac{9k}{9k^2-16} \log\left[\frac{4}{3k}\sqrt{\left|\frac{C_2}{C_1}\right|}\right]. \tag{4.35}$$

The curvature of the metric (4.33) is negative and reads

$$R = -\frac{5\mu^2}{\mathcal{C}^4}. \tag{4.36}$$

JHEP05(2019)117

Doing the change of coordinates

$$z = z_h \left(1 - e^{-2\mu u}\right)^{\frac{1}{4}}, \quad \mathcal{C} = z_h^{-2}, \tag{4.37}$$

one gets the usual form for the 5d AdS black brane

$$ds^2 = \frac{1}{z^2}\left(-f(z)dt^2 + d\vec{y}^2 + \frac{dz^2}{f(z)}\right), \tag{4.38}$$

with

$$f = 1 - \left(\frac{z}{z_h}\right)^4. \tag{4.39}$$

For the dilaton potential we have the saturation of the Gubser's bound (4.30)

$$V(\phi(u_h)) = V_{\rm UV}, \tag{4.40}$$

that is in agreement with the suggestion from [22], since the solution (4.33)–(4.35) is anti-de Sitter black brane.

One can summarize our studies on non-vacuum solutions as follows. For $u \to \pm\infty$ the scalar curvature and the dilaton for the right and left solutions can be constant for arbitrary value of the temperature which at the same time defines the constant E_2 (4.5). However, the left solutions have a special point u_{02} at which the scalar curvature has a non-removable singularity, while the scalar curvature of the right solutions is regular at its special point u_{01}. Finally, from (4.29) and (4.40) we see that the dilaton potential calculated on-shell is bounded only for the right solutions and special solutions with $u_{01} = u_{02}$. Therefore, these solutions can satisfy Gubser's criterion [22].

4.3 RG flow for non-vacuum solutions

4.3.1 Details of RG flow for vacuum solutions

In section 4 we showed that non-zero temperature solutions are characterized by the parameter $\alpha^1 \neq 0$. The scale factor of the domain wall for the finite temperature case (2.57) is

$$\mathcal{A} = \frac{1}{2}\log(\mathcal{C}) + \frac{1}{2}\log(\mathcal{X}) \tag{4.41}$$

and the energy scale A reads

$$\mathrm{A} \equiv e^{\mathcal{A}} = \mathcal{C}^{\frac{1}{2}}\mathcal{X}^{\frac{1}{2}}, \tag{4.42}$$

we note that to come to the domain wall form we use the change of the coordinate

$$dw = \mathcal{C}^2\,\mathcal{X}(u)^2 e^{\frac{8}{3}\alpha^1 u} du. \tag{4.43}$$

The finite temperature case is described by the additional variable Y defined through the blackening function (2.60). Here we deal with the system (2.61)–(2.62), which seems to be rather complicated comparing to the zero-T case and one has to apply analytic solutions for ϕ and $\mathcal{A}$ with the coordinate $u > u_{01}$ to show the RG flow.

JHEP05(2019)117

To see the behaviour of the RG flow at finite temperature it is useful to plot X and Y as functions of ϕ for the analytical solution. We remind the horizon of the black brane at $u \to +\infty$ in this case is defined for $\alpha^1 < 0$. In figure 16 we draw X and Y as functions of ϕ for different values of the negative α^1. From figure 16A we see that the behaviour of X is changed by α^1, so X becomes to be negative in the finite-T case. As for the Y function one can see from figure 16B that it is positive. In figure 16A we observe that the X function has stop points at some values of ϕ. These values of ϕ correspond to the asymptotics of the dilaton at the horizon ϕ_h (4.27). One can show that X given by

$$X = \frac{1}{3}\frac{\phi'}{\mathcal{A}'} \tag{4.44}$$

takes a constant value at the horizon with $u \to \infty$ as well and this can be observed as a stop point. For this let us trace the dependence of ϕ and $\mathcal{A}$ on u with $u \to +\infty$

$$\lim_{u\to+\infty} \phi = \frac{9k}{9k^2-16}\left(e^{-2\mu u} - e^{-2\mu(u-u_{02})}\right), \tag{4.45}$$

then we have

$$\lim_{u\to+\infty} \phi' = \frac{-18k\mu}{9k^2-16} e^{-2\mu u}\left(1 - e^{2\mu u_{02}}\right). \tag{4.46}$$

The scale factor for the black brane is given by (4.41) and have the following asymptotics at the horizon

$$\lim_{u\to+\infty} \mathcal{A} = \frac{1}{2}e^{-2\mu u}\left(\frac{16-9k^2e^{2\mu u_{02}}}{2(16-9k^2)}\right) + \frac{1}{2}\log(\mathcal{C}), \tag{4.47}$$

so we have

$$\lim_{u\to+\infty} \mathcal{A}' = -\mu\left(\frac{16-9k^2e^{2\mu u_{02}}}{2(16-9k^2)}\right)e^{-2\mu u}. \tag{4.48}$$

Then the value of X at the horizon is

$$\lim_{u\to+\infty} X = -12k\frac{e^{-2\mu u_{02}}-1}{16e^{-2\mu u_{02}}-9k^2}. \tag{4.49}$$

We see that

$$X \to 0, \tag{4.50}$$

as $\mu \to 0$.

As for the Y-function (2.60), it takes infinite values at the horizon that can be read from figure 16B.

In figure 17 we present the dependences of X and Y on the energy scale A. In figure 17A we again observe stop points of X at some $\mathcal{A}$ (4.47) with $u \to +\infty$.

JHEP05(2019)117

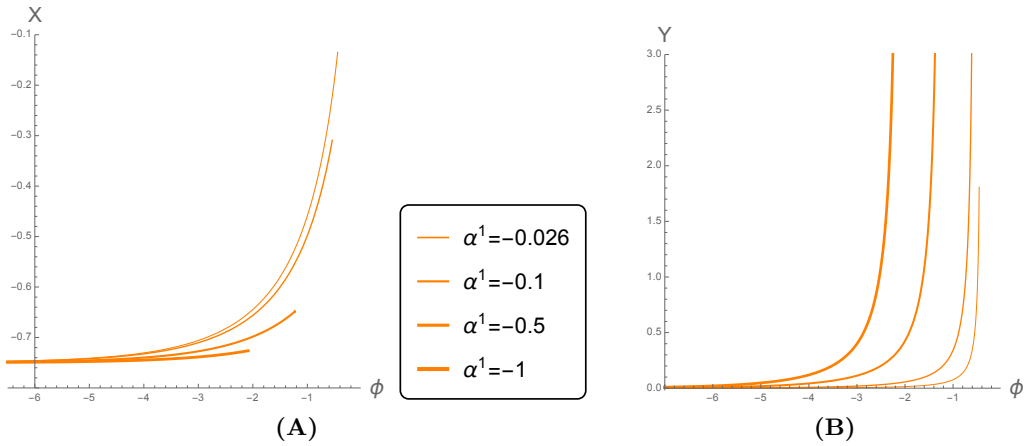

Figure 16. **A)** The dependence of the scalar function X on ϕ. **B)** The dependence of the scalar function Y on ϕ. For both plots $\alpha^1 < 0$, $u > u_{01}$, $C_1 = -C_2 = -2$, $k = 1$, $u_{01} = 0$, $u_{02} = -1$.

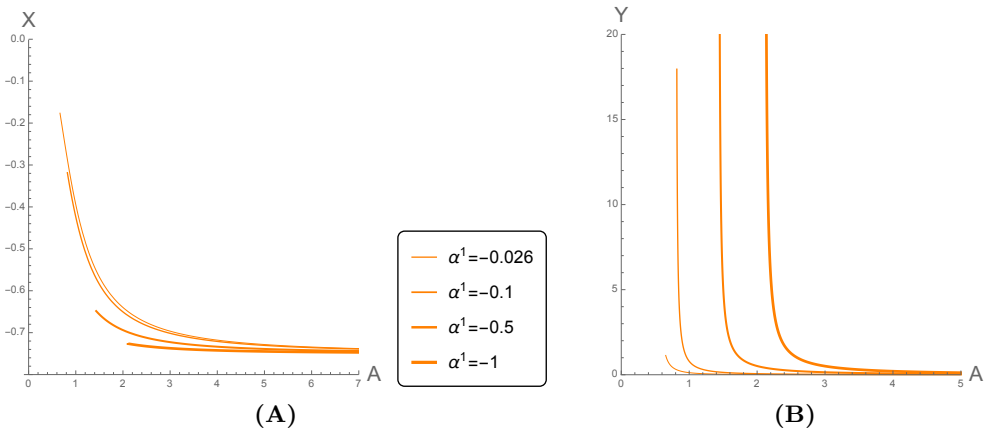

Figure 17. The RG flows for the right solution with $\alpha^1 < 0$. **A)** The flow in the (A, X) plane. **B)** The flow in the (A, Y) plane. For all $C_1 = -C_2 = -2$, $k = 1$, $u_{01} = 0$, $u_{02} = -1$.

4.3.2 The running coupling $\lambda = e^{\phi}$ on the energy scale for $T \neq 0$ flow

Now let us look what happens with the behaviour of the running coupling on the energy scale at finite temperature. As for the vacuum case we have the parametric dependence on E_1, E_2, α^1, the position of poles u_{01} and u_{02}. We note that E_1, E_2 and k are not independent. We have also seen before the temperature is related to the parameter α^1 (4.12). As in the previous section, section 3.3.2, to have an insight to possible behavior of the running coupling on the constructed solutions, we start with presenting the behavior of the energy scale A as a function of the coordinate u with (3.5)–(3.7) and then incorporated found in section 4, see figure 13, the behavior of the dilaton as a function of u.

In figure 18 we see that A tends to some constant value at $u \to \infty$ that can be supported by (4.47).

In figure 19 we present the parametric dependence of the running coupling λ as a function of the energy scale A for the black brane solutions with $u_{01} = 0$, $u_{02} = -1$ and

JHEP05(2019)117

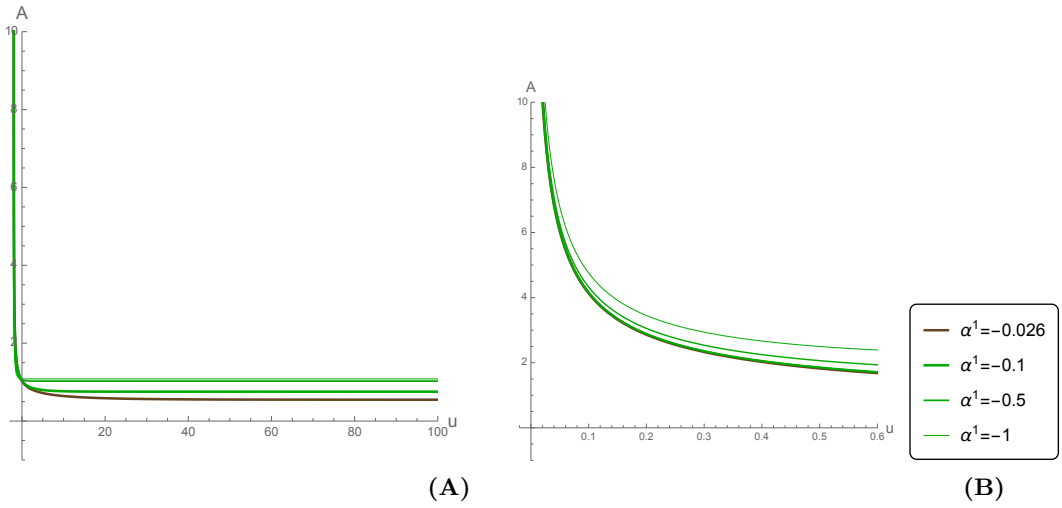

Figure 18. The plots show A for $u_{01} = 0$ and $u_{02} = -1$, $C_1 = -2$, $C_2 = 2$, $k = 1$ and negative α^1. The plot in the right panel zooms the area closed to zero of the left panel plot.

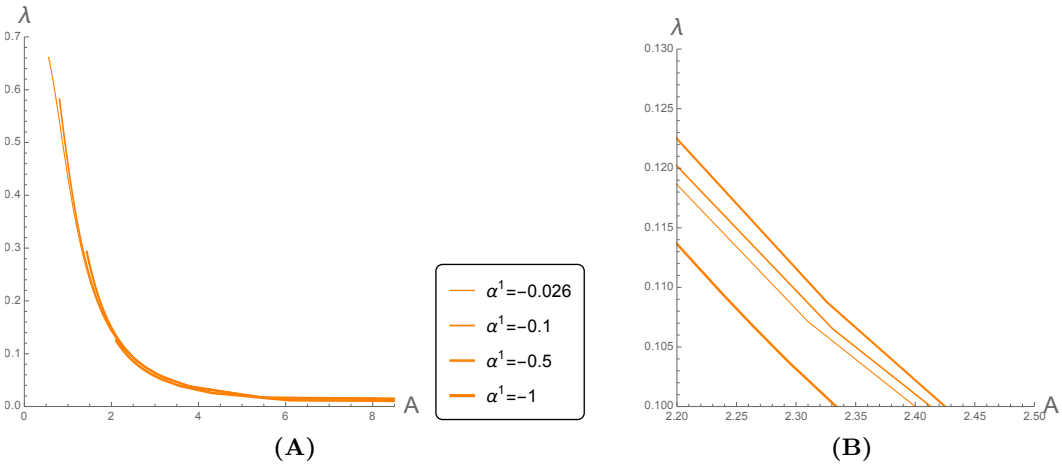

Figure 19. **A)** The dependence of λ on the energy scale A$= e^{\mathcal{A}}$. In all cases constants that the potential is fixed with $k = 1$, $C_1 = -2$, $C_2 = 2$ and we vary α^1, $u_{01} = 0$ and $u_{02} = -1$. **B)** A zoomed region of **A)**.

different values of the parameter α^1. We see that the IR dynamics is changed by α^1. This comes from the fact the dilaton can change the asymptotics from $-\infty$ to some constant value with (4.15) as has been explained in section 4. So we observe the increasing coupling constant in the IR regions. For A$\to +\infty$ the running coupling λ goes to 0 for all chosen parameters providing the UV freedom. Or in others words, we can mimic the QCD RG flow for negative α^1.

4.4 Free energy

The free energy corresponding to the black brane solution is given by the renormalized on-shell action. This can be computed directly, but the computation is simplified by the

JHEP05(2019)117

following observations. We use the domain wall coordinates here. First, the trace of the Einstein equations gives

$$R = \frac{5}{3}V + \frac{4}{3}(\partial\phi)^2, \tag{4.51}$$

so that the bulk Lagrangian on-shell is

$$\sqrt{g}\left(R - \frac{4}{3}(\partial\phi)^2 - V\right) = \frac{2}{3}e^{4\mathcal{A}}V\,. \tag{4.52}$$

The finite temperature potential equations imply that

$$V = -(12\mathcal{A}'^2 + 3\mathcal{A}'')f - 3\mathcal{A}'f'\,, \tag{4.53}$$

and from this relation one can see that the bulk term is a total derivative

$$\mathcal{L}_{\rm bulk} = -2\frac{d}{dw}(e^{4\mathcal{A}}\mathcal{A}'f)\,. \tag{4.54}$$

The normal vector to the cutoff surface $w = \epsilon$ is $n^w = \sqrt{f}, n^i = 0$. The extrinsic curvature reads

$$K = \frac{1}{2}h^{ab}n^w\partial_w h_{ab} = \frac{\sqrt{f}}{2}\left(8\mathcal{A}' + \frac{f'}{f}\right)\,. \tag{4.55}$$

The on-shell Einstein action with regularization

$$\begin{aligned} I_E^\epsilon &= -2V_3\int_0^\beta dt\int_\epsilon^{w_h} dw\frac{d}{dw}(e^{4\mathcal{A}}\mathcal{A}'f) \\ &= -2V_3\beta(e^{4\mathcal{A}(w_h)}\mathcal{A}'(w_h)f(w_h) - e^{4\mathcal{A}(\epsilon)}\mathcal{A}'(\epsilon)f(\epsilon)) \\ &= 2V_3\beta e^{4\mathcal{A}(\epsilon)}\mathcal{A}'(\epsilon)f(\epsilon), \end{aligned} \tag{4.56}$$

while the Gibbons-Hawking term with regularization reads

$$I_{\rm GH}^\epsilon = V_3\int_0^\beta dt\frac{fe^{4\mathcal{A}}}{2}\left[8\mathcal{A}' + \frac{f'}{f}\right]_\epsilon = V_3\beta e^{4\mathcal{A}(\epsilon)}(8\mathcal{A}'(\epsilon)f(\epsilon) + f'(\epsilon)), \tag{4.57}$$

so we get

$$\frac{I_{\rm reg}}{\beta V_3} = -e^{4\mathcal{A}}(6\mathcal{A}'f + f')|_{w=\epsilon}\,. \tag{4.58}$$

We need to evaluate it on the regular black brane solutions given by eqs. (4.17)–(4.19), and (4.26). Taking into account the change of coordinates $dw = e^{4\mathcal{A}}fdu$, the action becomes

$$\frac{I_{\rm reg}}{\beta V_3} = -\left(6\mathcal{A}'(u) + \frac{f'(u)}{f(u)}\right)\Big|_{u=\epsilon}\,. \tag{4.59}$$

The expansion of the scale factor $\mathcal{A}$ near $u \sim 0$ reads

$$\mathcal{A} \sim -\tfrac{4}{16-9k^2}\log u + \mathcal{A}_0 + \mathcal{A}_1 u + \dots\,, \tag{4.60}$$

with

$$\mathcal{A}_0 = \frac{1}{2}\log\mathcal{C} - \frac{4}{16-9k^2}\log(2\mu) + \frac{9k^2}{4(16-9k^2)}\log(1-e^{2\mu u_{02}}), \tag{4.61}$$

$$\mathcal{A}_1 = \frac{4\mu}{16-9k^2} + \frac{9k^2}{2(16-9k^2)}\frac{\mu}{e^{-2\mu u_{02}}-1}. \tag{4.62}$$

JHEP05(2019)117

Plugging (4.60) in (4.59) we obtain the regularised on-shell action

$$\begin{aligned}\frac{I_{\rm reg}}{\beta V_3} &= \frac{24}{16-9k^2}\frac{1}{\epsilon} - 6\mathcal{A}_1 + 2\mu \\ &= \frac{1}{16-9k^2}\left(\frac{24}{\epsilon} + \mu\left(8 - 18k^2 - \frac{27k^2}{e^{-2\mu u_{02}}-1}\right)\right).\end{aligned} \tag{4.63}$$

The regularized on-shell is divergent and one needs to add the counterterms before removing the cut-off.

The counterterms for the general dilaton-gravity system have been derived in [23]. For our homogeneous solutions the only relevant term is

$$I_{\rm ct} = -\frac{8}{3}\int d^4x\sqrt{h}\,U(\phi), \tag{4.64}$$

where U is any function that satisfies the equation of the zero-temperature superpotential. We use then the superpotential appropriate for the regular solution, i.e. (see appendix C)

$$I_{\rm ct} = -\frac{8\gamma}{3}\int d^4x\sqrt{h}e^{k\phi}\,. \tag{4.65}$$

The asymptotics of the dilaton is given by

$$\phi \sim \frac{9k}{16-9k^2}\log u + \phi_0 + \phi_1 u + \dots \tag{4.66}$$

with

$$\phi_0 = -\frac{9k}{16-9k^2}\log\left(\frac{4}{3k}\sqrt{\frac{C_2}{C_1}}\frac{\sinh(-\mu u_{02})}{\mu}\right), \tag{4.67}$$

$$\phi_1 = -\frac{9k}{16-9k^2}\mu\coth(-\mu u_{02})\,. \tag{4.68}$$

Using the asymptotics (4.60)–(4.62) and (4.66)–(4.68) we find

$$\mathcal{L}_{\rm ct} = -\frac{24}{16-9k^2}\left(\frac{1}{\epsilon} + 4\mathcal{A}_1 + k\phi_1\right)(1-\mu\epsilon) = -\frac{24}{16-9k^2}\frac{1}{\epsilon} + o(\epsilon)\,. \tag{4.69}$$

The renormalized action is then

$$\begin{aligned}\frac{I_{\rm ren}}{\beta V_3} &= \frac{I_{\rm reg}+I_{\rm ct}}{\beta V_3} = \frac{\mu}{16-9k^2}\left(8-18k^2-\frac{27k^2}{e^{-2\mu u_{02}}-1}\right) = \\ &= \frac{1}{2}\left(\mu - \frac{27k^2}{16-9k^2}\sqrt{\Lambda^2+\mu^2}\right),\end{aligned} \tag{4.70}$$

where we defined the UV scale in terms of the scale factor at the boundary, i.e. by setting

$$\frac{\mu}{\Lambda} = \sinh(-\mu u_{02})\,. \tag{4.71}$$

JHEP05(2019)117

The free energy can be computed through the renormalized on-shell action (4.70); the difference between the free energy of the black brane solution and the free energy of the vacuum, obtained at $\mu = 0$, is

$$\mathcal{F} \sim -\frac{1}{2}\left(\mu - \frac{27k^2}{16-9k^2}(\sqrt{\Lambda^2+\mu^2}-\Lambda)\right). \tag{4.72}$$

On the other hand one can calculate the free energy using black brane thermodynamics, that involves the following relation for the free energy, the entropy density and the temperature of the black brane

$$d\mathcal{F} = -s dT. \tag{4.73}$$

At the same time the black brane entropy density reads

$$s = \frac{1}{4}\int \sqrt{h_{\rm ind}}\, dy_1 dy_2 dy_3\Big|_{u\to\infty}, \tag{4.74}$$

since $\mathcal{X} \to 1$ at the horizon we have

$$s = \frac{V_3}{4}\,\mathcal{C}^{\frac{3}{2}}. \tag{4.75}$$

Comparing (4.75) with (4.16) and taking into account the relation

$$\mu = -\frac{4\alpha^1}{3}, \tag{4.76}$$

we get

$$s\,T = \frac{V_3}{2\pi}\,\mu. \tag{4.77}$$

Integrating (4.73) we get the expression for the free energy

$$\mathcal{F} = -\int s\, dT = -\frac{V_3}{2\pi}\int_0^\mu \frac{\mu'}{T}\frac{dT}{d\mu'}\, d\mu'. \tag{4.78}$$

The temperature as function of μ is

$$T = \frac{2}{3\pi Q^{3/2}}\left|\frac{3}{4}\mu\right|^{1/4} e^{\frac{27k^2}{4(16-9k^2)}\,u_{02}\,\mu}, \tag{4.79}$$

but we have to express u_{02} in terms of the scale Λ, using (4.71); we get

$$T = \frac{\sqrt{2}}{3^{3/4}\pi Q^{3/2}}\mu^{1/4} e^{-\frac{27k^2}{4(16-9k^2)}\,\mathrm{arcsinh}\left(\frac{\mu}{\Lambda}\right)}. \tag{4.80}$$

Performing integration in (4.78) with T given by (4.80) we obtain for the free energy

$$\mathcal{F} = -\frac{V_3}{8\pi}\left(\mu - \frac{27k^2}{16-9k^2}(\sqrt{\Lambda^2+\mu^2}-\Lambda)\right), \tag{4.81}$$

in agreement with the result from the renormalized action.

JHEP05(2019)117

The temperature and the free energy exhibit a qualitatively different behavior depending on the value of k. In the case $0 < k < \frac{2}{3}$, both are monotonic functions, so the black brane solution exists for any temperature, and there is no phase transition, so the black brane is thermodynamically favored over the thermal gas solution.

In the other case, for $\frac{2}{3} < k < \frac{4}{3}$, the temperature increases as function of μ up to a maximum value and then decreases back to zero. The maximum is attained at

$$\frac{\mu_{\max}}{\Lambda} = \frac{16 - 9k^2}{\sqrt{8(9k^2-4)(9k^2+8)}}\,. \tag{4.82}$$

The free energy is initally negative, but changes sign at

$$\frac{\mu_{cr}}{\Lambda} = \frac{54k^2(16-9k^2)}{8(9k^2-4)(9k^2+8)} > \frac{\mu_{\max}}{\Lambda}\,. \tag{4.83}$$

We notice that considering $u_{02} \to 0$, we get $\Lambda \to 0$ and the free energy comes to

$$\mathcal{F} = -\frac{V_3}{8\pi}\mu \tag{4.84}$$

the dependence on the scale disappears, consistently with the fact that the solution becomes the AdS black brane, with the constant dilaton, and there is no phase transition.

In figure 20 we present the behaviour of the free energy on the temperature for different values of k. As we discussed above for $0 < k < \frac{2}{3}$ the free energy is monotonic, while for $\frac{2}{3} < k < \frac{4}{3}$ the free energy decreases up to $T_{\max}$ and then starts to increase, while the temperature is decreasing. This phase diagram cannot be complete, as the free energy would be discontinuous at $T_{\max}$. We do not know whether this means that the dual theory does not make sense for this range of k, or there is some other solution that connects to the ones that we know and restores the continuity. It is worth to notice that a similar behaviour of the free energy was observed in [24] for black hole solutions which are the finite temperature generalizations of the bouncing vacuum solutions.

5 Conclusion and discussion

We have presented some analytic solutions of Einstein equations coupled to a dilaton field, at zero and non-zero temperatures, that correspond to holographic RG flows between different fixed points. The non-trivial form of the potential allows for a rich variety of different behaviours for the dilaton and the scale factor, corresponding to a coupling that can run to zero or to infinity in the UV and in the IR. We mainly considered solutions which are governed by sinh-functions. However we have two more classes of solutions for our choice of the potential, namely the sin-class and linear class. All solutions depend on two parameters, u_{01} and u_{02}, splitting the solutions into three branches: "left", "middle" and "right". Moreover, a special solution appears when $u_{01} = u_{02}$. In the zero-temperature case the dilaton flows from $+\infty$ to $-\infty$ both for the left and middle solutions. However, the scale factor of the left solution is non-monotonic function while the scale factor of the middle solution monotonically decreases. Correspondingly, the left vacuum solution

JHEP05(2019)117

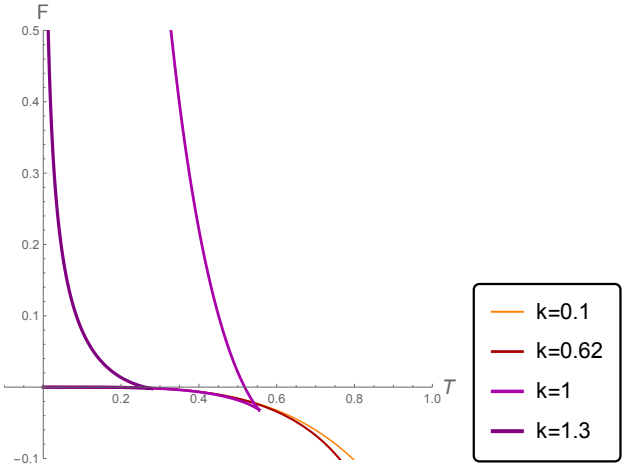

Figure 20. The dependence of the free energy F on the temperature T for the different shapes of the potential (different k, $C_1 = -2$, $C_2 = 2$).

does not have a holographic interpretation and the middle one is supposed to describe a holographic RG flow that mimics QCD behaviour. The right solution at $T = 0$ has a bouncing dilaton and a scale factor, that monotonically decreases, i.e. it has both IR and UV free limits. We note that the left, middle and right solutions interpolate between the hyperscaling violating boundaries. A special family of solutions with $u_{01} = u_{02}$ interpolates between an AdS boundary in the UV limit given by (3.28) and the hyperscaling violating boundary in the IR limit. Another solution with an AdS boundary but in the IR limit (and the hyperscaling violating boundary in the UV limit) is the one from the linear class. For the right vacuum solution we could find its black brane analogue, which again interpolates between the hyperscaling violating boundaries with a constant dilaton at the horizon. The special solution with coinciding point turns to be AdS-Schwarzschild black hole with the corresponding constant dilaton. We also showed that the finite temperature solutions can behave very differently from the corresponding zero-temperature ones.

The next step in our program is to understand better these solutions from the point of view of the putative dual field theory. From the phenomenological perspective, we would like to be able to apply our model to real QCD (or Yang-Mills, since we do not introduce quarks). As mentioned in the introduction, the model with a single exponential has undesirable features in this respect. It corresponds to a dual theory with a beta function that is linear in the coupling. The model studied in this paper is an improvement in this direction, since some of the flows describe a theory that is asymptotically free in the UV, with a scale Λ, determined by the boundary conditions of the fields, that can be thought of as $\Lambda_{\rm QCD}$, and the coupling grows large in the IR.

It would be interesting to determine the spectrum of fluctuations around these solutions, in particular the quasi-normal modes of the black brane solutions, and also to extend our ansatz in order to look for analytic time dependent solutions that describe out-of-equilibrium dynamics.

It would also be worthwile to understand if the method we used, that reduces the Einstein equations to an integrable Toda chain, could be used for other case. In the

JHEP05(2019)117

model of two-exponential potentials that we used, there is a constraint (2.21)–(2.22) on the exponents of the potential; this restricts considerably the space of parameters that we can explore. We plan to consider extensions of the present work to different forms of the potential. For instance, [25] considers a potential with three exponential functions, that can appear after a reduction in the bosonic sector of gauged supergravity (a study of black holes for a particular case of such a potential was done in [26]). Having more terms in the potential allows us to have a richer landscape of critical points, including also de Sitter solutions in addition to AdS and hyperscaling geometries. In general, we would like to have a classification of all cases that can be solved with the techniques used here. One way to approach this problem could be to reverse-engineer the dilaton potential and understand if it can come from some dimensional reduction.

It would also be interesting to consider the coupling of a Maxwell field in the bulk and find charged black hole solutions.

Acknowledgments

We thank E. Kiritsis for valuable discussions and suggestions. GP would like to thank M. Jarvinen and F. Nitti for giving useful suggestions, and the Steklov Mathematical Institute for hospitality during the initial stages of this work. AG thanks Gleb Arutyunov, Eoin Ó Colgáin, Bum-Hoon Lee, Chanyong Park and Sunyoung Shin for useful conversations. AG is also very grateful for the warm hospitality DESY Theory Group, APCTP (Pohang) and Sogang University (Seoul). I.A. is supported by the "BASIS" Science Foundation (grant No. 18-1-1-80-4).

A The curvature invariants of the background

The ansatz for the metric is given by

$$ds^2 = -e^{2A(u)}dt^2 + e^{2B(u)}\sum_{i=1}^{3} dy_i^2 + e^{2C(u)}du^2. \tag{A.1}$$

The non-zero components of the Ricci tensor are

$$R_{00} = e^{2(A-C)}\left((\dot{A})^2 + 3\dot{A}\dot{B} - \dot{A}\dot{C} + \ddot{A}\right), \tag{A.2}$$

$$R_{11} = R_{22} = R_{33} = -e^{2(B-C)}\left(\dot{A}\dot{B} + 3\dot{B}^2 - \dot{B}\dot{C} + \dot{B}\right), \tag{A.3}$$

$$R_{44} = -\dot{A}^2 - 3\dot{B}^2 + \left(\dot{A} + 3\dot{B}\right)\dot{C} - \ddot{A} - 3\ddot{B}. \tag{A.4}$$

The scalar curvature reads

$$R = -2e^{-2C}\left[\dot{A}^2 + 3\dot{A}\dot{B} + 6(\dot{B})^2 - \dot{A}\dot{C} - 3\dot{B}\dot{C} + \ddot{A} + 3\ddot{B}\right]. \tag{A.5}$$

Thus, we have

$$\sqrt{|g|}R = -e^{A+3B-C}\left[2(\dot{A})^2 + 6\dot{A}\dot{B} + 12(\dot{B})^2 - 2\dot{A}\dot{C} - 6\dot{B}\dot{C} + 2\ddot{A} + 6\ddot{B}\right]. \tag{A.6}$$

JHEP05(2019)117

To find the solutions to the model we use the gauge $C = A+3B$ for (A.1). The generic form of the obtained solutions is

$$e^A = e^{A_1} e^{\alpha^1 u}, \quad e^B = e^{B_1} e^{-\frac{1}{3}\alpha^1 u}, \tag{A.7}$$

where the functions $A_1 = B_1$ and α^1 is a constant, which is equal to zero for the vacuum case. Now the scalar curvature (A.5) reads

$$R = -\frac{4}{3}\left((\alpha^1)^2 - 9\dot{A}_1^2 + 6\ddot{A}_1\right) e^{-8A_1}, \tag{A.8}$$

that covers the vacuum case with $\alpha^1 = 0$

$$R = \left(12\dot{A}_1^2 - 8\ddot{A}_1\right) e^{-8A_1}. \tag{A.9}$$

The Kretschmann scalar is defined as follows

$$K = R_{abcd} R^{abcd}. \tag{A.10}$$

Pluggin the metric (A.1) we have

$$\begin{aligned} K = {} & 4(\dot{A}^4 + 3\dot{A}^2\dot{B}^2 + 6\dot{B}^4 + 2\dot{A}^2\ddot{A} + 6\dot{B}^2\ddot{B} + (\dot{A}^2 + 3\dot{B}^2)\dot{C}^2 + \ddot{A}^2 + 3\ddot{B}^2 \\ & -2(\dot{A}^3 + 3\dot{B}^3 + \dot{A}\ddot{A} + 3\dot{B}\ddot{B})\dot{C})e^{-4C}. \end{aligned} \tag{A.11}$$

One can write down the Kretschmann scalar of the non-vacuum solution ($\alpha^1 \neq 0$)

$$K = \frac{8}{27}\left((\alpha^1 - 3\dot{A}_1)^2(19\alpha^1 + 42\alpha^1\dot{A}_1 + 63\dot{A}_1^2) + 36(\alpha^1 - 9\dot{A}_1^2)\ddot{A}_1 + 54\ddot{A}_1^2\right) e^{-16A_1}. \tag{A.12}$$

Taking into account that $C = 4A_1$ and $\alpha^1 = 0$ for the vacuum solution one obtains

$$K = 8(21\dot{A}_1^4 - 12\dot{A}_1^2\ddot{A}_1 + 2\ddot{A}_1^2)e^{-16A_1}. \tag{A.13}$$

A.1 The equations of motion in the harmonic gauge

The Einstein equations of motion which follow from the action with the harmonic gauge $A + 3B = C$ are

$$e^{-6B}\left[3B'^2 + 3A'B' - 3B''\right] = \frac{2}{3}\phi'^2 e^{-6B} + \frac{1}{2}e^{2A}V, \tag{A.14}$$

$$e^{-2A-4B}\left[-3B'^2 - 3A'B' + \frac{\partial^2 A}{\partial u^2} + 2B''\right] = -\frac{2}{3}\phi'^2 e^{-2A-4B} - \frac{1}{2}e^{2B}V, \tag{A.15}$$

$$3B'^2 + 3B'A' = \frac{2}{3}\phi'^2 - \frac{1}{2}e^{2A+6B}V \tag{A.16}$$

and the dilaton equation of motion reads

$$\frac{8}{3}e^{-2A-6B}\phi'' - V'_\phi = 0. \tag{A.17}$$

JHEP05(2019)117

A.2 The scalar curvature of the vacuum solutions

Using the expression for the scalar curvature (A.9) and taking into account (2.43) and (2.48)–(2.49) one can write

$$
\begin{aligned}
R = & \frac{(C_1/2E_1)^{\frac{16}{16-9k^2}}(C_2/2E_2)^{\frac{-9k^2}{16-9k^2}}}{4(16-9k^2)^2}\Big(8(16-9k^2)(16\mu_1^2-9k^2\mu_2^2) \\
& +128(9k^2-10)\mu_1^2\coth(\mu_1(u-u_{01}))^2 \\
& -864k^2\mu_1\mu_2\coth(\mu_1(u-u_{01}))\coth(\mu_2(u-u_{02})) \\
& +9k^2(128-45k^2)\mu_2^2\coth(\mu_2(u-u_{02}))^2\Big)\sinh(\mu_1(u-u_{01}))^{\frac{32}{16-9k^2}}\sinh(\mu_2(u-u_{02}))^{\frac{-18k^2}{16-9k^2}}.
\end{aligned}
\tag{A.18}
$$

It is exemplarily to look how the scalar curvature behaves for each branch of the solution.

- For the left solution which is defined for $u < u_{02}$ we have the following limits
  - $u \to -\infty$, so (A.18) can be rewritten as

$$
R = \left(\frac{C_1}{2E_1}\right)^{\frac{16}{16-9k^2}}\left(\frac{C_2}{2E_2}\right)^{-\frac{9k^2}{16-9k^2}}\frac{3(16\mu_1-9k^2\mu_2)^2}{4(16-9k^2)^2}e^{-\frac{2(16\mu_1-9k^2\mu_2)}{16-9k^2}u}. \tag{A.19}
$$

    The quantity $(16\mu_1-9k^2\mu_2)$, with $\mu_1=\sqrt{\left|\frac{3E_1}{2}\left(k^2-\frac{16}{9}\right)\right|}$, $\mu_2=\sqrt{\left|\frac{3E_2}{2}\left(\left(\frac{16}{9}\right)^2\frac{1}{k^2}-\frac{16}{9}\right)\right|}$, $|E_1| = |E_2|$, $0 < k < 4/3$ is always positive and the scalar curvature grows as $u \to -\infty$.

    The scalar curvature in the conformal coordinates with $z \to 0$

$$
R = \left(\frac{C_1}{2E_1}\right)^{\frac{16}{16-9k^2}}\left(\frac{C_2}{2E_2}\right)^{-\frac{9k^2}{16-9k^2}}\frac{3(16\mu_1-9k^2\mu_2)^2}{4(16-9k^2)^2}\left(\frac{3\mu_1}{4+3k}z\right)^{-\frac{8}{3}}. \tag{A.20}
$$

  - $u \to u_{02}-\epsilon$, then the scalar curvature (A.18) takes the form

$$
\begin{aligned}
R = & \frac{(C_1/2E_1)^{\frac{16}{16-9k^2}}(C_2/2E_2)^{\frac{-9k^2}{16-9k^2}}}{4(16-9k^2)^2}\Big(8(16-9k^2)(16\mu_1^2-9k^2\mu_2^2) \\
& +128(9k^2-10)\mu_1^2\coth(\mu_1(u_{02}-u_{01}))^2-864k^2\mu_1\coth(\mu_1(u_{02}-u_{01}))(u-u_{02})^{-1} \\
& +9k^2(128-45k^2)(u-u_{02})^{-2}\Big)\sinh(\mu_1(u_{02}-u_{01}))^{\frac{32}{16-9k^2}}(\mu_2(u-u_{02}))^{\frac{-18k^2}{16-9k^2}},
\end{aligned}
\tag{A.21}
$$

    where one can see that the scalar curvature (A.21) has divergencies. In the conformal coordinates the scalar curvature at $u \to u_{02}-\epsilon$ is

$$
\begin{aligned}
R = & \frac{(C_1/2E_1)^{\frac{16}{16-9k^2}}(C_2/2E_2)^{\frac{-9k^2}{16-9k^2}}}{4(16-9k^2)^2}\Big(8(16-9k^2)(16\mu_1^2-9k^2\mu_2^2) \\
& +128(9k^2-10)\mu_1^2\coth(\mu_1(u_{02}-u_{01}))^2
\end{aligned}
$$

JHEP05(2019)117

$$
\begin{aligned}
&-864k^2\mu_1\coth(\mu_1(u_{02}-u_{01}))\left(\frac{4(16-9k^2)}{64-9k^2}z\right)^{\frac{4(16-9k^2)}{9k^2-64}}\\
&+9k^2(128-45k^2)\left(\frac{4(16-9k^2)}{64-9k^2}z\right)^{\frac{8(16-9k^2)}{9k^2-64}}\Bigg)\\
&\cdot\sinh(\mu_1(u_{02}-u_{01}))^{\frac{32}{16-9k^2}}\left(\mu_2\frac{4(16-9k^2)}{64-9k^2}z\right)^{\frac{72k^2}{9k^2-64}}.
\end{aligned}
\tag{A.22}
$$

- The middle solution with $u\in(u_{01};u_{02})$ can be characterized by the following limits
  - for $u\to u_{02}+\epsilon$ the scalar curvature is the same as for the left solution (A.21)–(A.22), so divergencies as (A.21) for the left solution.
  - $u\to u_{01}-\epsilon$, so (A.18) reads as

$$
\begin{aligned}
R=\frac{(C_1/2E_1)^{\frac{16}{16-9k^2}}(\sqrt{C_2/2E_2}\sinh(\mu_2(u_{01}-u_{02})))^{\frac{-18k^2}{16-9k^2}}}{4(16-9k^2)^2}\Big(&8(16-9k^2)(16\mu_1^2-9k^2\mu_2^2)\\
&+128(9k^2-10)(|u-u_{01}|)^{-2}-864k^2\mu_2(|u-u_{01}|)^{-1}\coth(\mu_2(u_{01}-u_{02}))\\
&+9k^2(128-45k^2)\mu_2^2\coth(\mu_2(u_{01}-u_{02}))^2\Big)(\mu_1(u_{01}-u))^{\frac{32}{16-9k^2}},
\end{aligned}
\tag{A.23}
$$

that is regular. As for the scalar curvature written in the conformal coordinates

$$
\begin{aligned}
R=\frac{(C_1/2E_1)^{\frac{16}{16-9k^2}}(\sqrt{C_2/2E_2}\sinh(\mu_2(u_{01}-u_{02})))^{\frac{-18k^2}{16-9k^2}}}{4(16-9k^2)^2}&\left(128(9k^2-10)\left(\frac{9k^2-4}{16-9k^2}z\right)^{\frac{2(16-9k^2)}{9k^2-4}}\right.\\
&-864k^2\mu_2\left(\frac{9k^2-4}{16-9k^2}z\right)^{\frac{16-9k^2}{9k^2-4}}\coth(\mu_2(u_{01}-u_{02}))\\
&\left.+9k^2(128-45k^2)\mu_2^2\coth(\mu_2(u_{01}-u_{02}))^2\right)\left(\mu_1\frac{9k^2-4}{16-9k^2}z\right)^{\frac{32}{4-9k^2}},
\end{aligned}
\tag{A.24}
$$

where z is given by (3.17).

- For the right solution one has
  - $u\to u_{01}+\epsilon$ The scalar curvature matches with that one (A.23)–(A.24) for the middle solution near the point u_{01}.
  - $u\to+\infty$

$$
R=\left(\frac{C_1}{2E_1}\right)^{\frac{16}{16-9k^2}}\left(\frac{C_2}{2E_2}\right)^{-\frac{9k^2}{16-9k^2}}\frac{3(16\mu_1-9k^2\mu_2)^2}{4(16-9k^2)^2}e^{\frac{2(16\mu_1-9k^2\mu_2)}{16-9k^2}u}.
\tag{A.25}
$$

JHEP05(2019)117

As for the left solution the scalar curvature (A.25) grows due to $(16\mu_1 - 9k^2\mu_2) > 0$ as for (A.19) with $u \to -\infty$. In the conformal coordinates (A.25) is

$$R = \left(\frac{C_1}{2E_1}\right)^{\frac{16}{16-9k^2}} \left(\frac{C_2}{2E_2}\right)^{-\frac{9k^2}{16-9k^2}} \frac{3(16\mu_1 - 9k^2\mu_2)^2}{4(16-9k^2)^2} \left(\frac{3\mu_1}{4+3k} z\right)^{-\frac{8}{3}}, \quad \text{(A.26)}$$

with $z \to 0$.

- Let's find the scalar curvature for the special case of the solution with $u_{01} = u_{02} = u_0$.

  The general formula for the scalar curvature with $u_{01} = u_{02} = u_0$ reads

$$R = \frac{\left(\sqrt{\frac{C_1}{2E_1}} \sinh(\mu_1(u-u_{01}))\right)^{\frac{32}{16-9k^2}} \left(\sqrt{\frac{C_2}{2E_2}} \sinh(\mu_2(u-u_{01}))\right)^{\frac{18k^2}{-16+9k^2}}}{4(16-9k^2)^2} \cdot \Big(8(9k^2-16)(9k^2\mu_2^2-16\mu_1^2)$$
$$+128(-10+9k^2)\mu_1^2 \coth^2(\mu_1 u) - 864k^2\mu_1\mu_2 \coth(\mu_1 u)\coth(\mu_2 u)$$
$$+9k^2(128-45k^2)\mu_2^2 \coth^2(\mu_2 u)\Big). \quad \text{(A.27)}$$

  Here one has to study the behaviour of the scalar curvature in the limits of small u and $u \to +\infty$.

  For $u \to u_0$ one has

$$R = -\frac{5}{4}\left(\sqrt{\frac{C_1}{2E_1}}\mu_1\right)^{\frac{32}{16-9k^2}} \left(\sqrt{\frac{C_2}{2E_2}}\mu_2\right)^{\frac{18k^2}{9k^2-16}}. \quad \text{(A.28)}$$

  So, one comes to a background with the constant negative curvature in the case of small values of u.

  For $u \to +\infty$ we onbtain

$$R = \frac{3}{4}\frac{(16\mu_1 - 9k^2\mu_2)^2}{(16-9k^2)^2} \left(\frac{C_1}{2E_1}\right)^{\frac{32}{16-9k^2}} \left(\frac{C_2}{2E_2}\right)^{\frac{18k^2}{-16+9k^2}} e^{\frac{2(16\mu_1-9k^2\mu_2)}{16-9k^2}u}, \quad \text{(A.29)}$$

  that is an agreement with (A.25). The corresponding expression in the scalar coordinates matches with (A.26).

A.3 The scalar curvature of the non-vacuum solutions

Now we turn to the non-vacuum background (4.1) with (4.2)–(4.3), which is characterized by a non-zero parameter α^1. The scalar curvature for the non-vacuum case reads

$$R = -\Big(8(9k^2-16)\left(\frac{2}{3}(\alpha^1)^2(9k^2-16)+16\mu_1^2-9k^2\mu_2^2\right)+128(10-9k^2)\mu_1^2\coth(\mu_1(u-u_{01}))^2$$
$$-864k^2\mu_1\mu_2\coth(\mu_1(u-u_{01}))\coth(\mu_2(u-u_{02}))+9k^2(-128+45k^2)\mu_2^2\coth^2(\mu_2(u-u_{02}))\Big)$$
$$\cdot\frac{\left(\sqrt{\frac{C_1}{2E_1}}\sinh(\mu_1(u-u_{01}))\right)^{\frac{32}{16-9k^2}}\left(\sqrt{\frac{C_2}{2E_2}}\sinh(\mu_2(u-u_{02}))\right)^{\frac{18k^2}{9k^2-16}}}{4(16-9k^2)^2}. \quad \text{(A.30)}$$

As for the vacuum solution it is instructive to see the scalar curvature for each of the branches with certain limits.

JHEP05(2019)117

- The left solution with $u < u_{02}$ has the following scalar curvature

  - $u \to -\infty$ one has

$$R = \left(\frac{C_1}{2E_1}\right)^{\frac{16}{16-9k^2}} \left(\frac{C_2}{2E_2}\right)^{-\frac{9k^2}{16-9k^2}} \left(\frac{3(16\mu_1 - 9k^2\mu_2)^2}{4(16-9k^2)^2} - \frac{4}{3}\left(\alpha^1\right)^2\right) e^{-\frac{2(16\mu_1-9k^2\mu_2)}{16-9k^2}u}. \tag{A.31}$$

  - For the limit $u \to u_{02} - \epsilon$

$$\begin{aligned} R = &-\left(8(9k^2-16)\left(\frac{2}{3}(\alpha^1)^2(9k^2-16)+16\mu_1^2-9k^2\mu_2^2\right)\right. \\ &+128(10-9k^2)\mu_1^2\coth(\mu_1(u_{01}-u_{02}))^2 \\ &\left.-864k^2\mu_1\coth(\mu_1(u_{01}-u_{02}))(u-u_{02})^{-1}+9k^2(-128+45k^2)(u-u_{02})^{-2}\right) \\ &\cdot\frac{\left(\sqrt{\frac{C_1}{2E_1}}\sinh(\mu_1(u_{01}-u_{02}))\right)^{\frac{32}{16-9k^2}}\left(\sqrt{\frac{C_2}{2E_2}}\mu_2(u-u_{02})\right)^{\frac{18k^2}{9k^2-16}}}{4(16-9k^2)^2}, \end{aligned} \tag{A.32}$$

    as for the vacuum case (A.21) the scalar curvature is divergent at u_{02}.
    In the conformal coordinates (A.32) reads

$$\begin{aligned} R = &-\left(8(9k^2-16)\left(\frac{2}{3}(\alpha^1)^2(9k^2-16)+16\mu_1^2-9k^2\mu_2^2\right)\right. \\ &+128(10-9k^2)\mu_1^2\coth(\mu_1(u_{01}-u_{02}))^2 \\ &-864k^2\mu_1\coth(\mu_1(u_{01}-u_{02}))\left(\frac{4(16-9k^2)}{64-9k^2}z\right)^{\frac{4(16-9k^2)}{9k^2-64}} \\ &\left.+9k^2(-128+45k^2)\left(\frac{4(16-9k^2)}{64-9k^2}z\right)^{\frac{8(16-9k^2)}{9k^2-64}}\right) \\ &\cdot\frac{\left(\sqrt{\frac{C_1}{2E_1}}\sinh(\mu_1(u_{01}-u_{02}))\right)^{\frac{32}{16-9k^2}}\left(\sqrt{\frac{C_2}{2E_2}}\mu_2\frac{4(16-9k^2)}{64-9k^2}z\right)^{\frac{72k^2}{9k^2-64}}}{4(16-9k^2)^2}. \end{aligned} \tag{A.33}$$

- The middle solution defined for $u \in (u_{01}; u_{02})$.

  - For $u \to u_{02}+\epsilon$ the scalar curvature matches with the curvature given by (A.32). As well as in the conformal coordinates it is the same as (A.33).

    One can seem that scalar curvature of the middle solution in the non-vacuum case has also a singularity at u_{01}.

JHEP05(2019)117

– $u \to u_{01} - \epsilon$

$$R = -\left(8(9k^2-16)\left(\frac{2}{3}(\alpha^1)^2(9k^2-16)+16\mu_1^2-9k^2\mu_2^2\right)+128(10-9k^2)(u-u_{01})^{-2}\right.$$
$$-864k^2\mu_2(u-u_{01})^{-1}\coth(\mu_2(u_{01}-u_{02}))$$
$$\left.+9k^2(-128+45k^2)\mu_2^2\coth^2(\mu_2(u_{01}-u_{02}))\right)$$
$$\cdot\frac{\left(\sqrt{\frac{C_1}{2E_1}}\mu_1(u-u_{01})\right)^{\frac{32}{16-9k^2}}\left(\sqrt{\frac{C_2}{2E_2}}\sinh(\mu_2(u_{01}-u_{02}))\right)^{\frac{18k^2}{9k^2-16}}}{4(16-9k^2)^2}, \tag{A.34}$$

or in the conformal coordinates with z given by (3.17)

$$R = -\left(8(9k^2-16)\left(\frac{2}{3}(\alpha^1)^2(9k^2-16)+16\mu_1^2-9k^2\mu_2^2\right)\right.$$
$$+128(10-9k^2)\left(\frac{9k^2-4}{16-9k^2}z\right)^{\frac{2(16-9k^2)}{9k^2-4}}-864k^2\mu_2\left(\frac{9k^2-4}{16-9k^2}z\right)^{\frac{16-9k^2}{9k^2-4}}\coth(\mu_2(u_{01}-u_{02}))$$
$$\left.+9k^2(-128+45k^2)\mu_2^2\coth^2(\mu_2(u_{01}-u_{02}))\right)$$
$$\cdot\frac{\left(\sqrt{\frac{C_1}{2E_1}}\mu_1\right)^{\frac{32}{16-9k^2}}\left(\frac{9k^2-4}{16-9k^2}z\right)^{\frac{32}{4-9k^2}}\left(\sqrt{\frac{C_2}{2E_2}}\sinh(\mu_2(u_{01}-u_{02}))\right)^{\frac{18k^2}{9k^2-16}}}{4(16-9k^2)^2}. \tag{A.35}$$

- The right solution with $u > u_{01}$
  - $u \to u_{01} + \epsilon$ the scalar curvature coincides with (A.34)–(A.35).
  - $u \to +\infty$

$$R = \left(\frac{C_1}{2E_1}\right)^{\frac{16}{16-9k^2}}\left(\frac{C_2}{2E_2}\right)^{-\frac{9k^2}{16-9k^2}}\left(\frac{3(16\mu_1-9k^2\mu_2)^2}{4(16-9k^2)^2}-\frac{4}{3}\left(\alpha^1\right)^2\right)e^{\frac{2(16\mu_1-9k^2\mu_2)}{16-9k^2}u}. \tag{A.36}$$

It should be noted that the scalar curvatures given by (A.31) and (A.26) can be equal to zero if the parameter α^1 is taken as

$$\alpha^1 = \pm\sqrt{\frac{(16-9k^2)E_2}{6k^2}}. \tag{A.37}$$

A.4 The Kretschmann scalar for the solution with $u > u_{01}$

For the vacuum solution defined for $u > u_{01}$ (the right solution) with $u \to u_{01} + \epsilon$ one has

$$K \sim k_0(u-u_{01})^{\frac{64}{16-9k^2}}\sum_{i=0}^{4}c_i(u-u_{01})^{-i}, \tag{A.38}$$

where k_0 and c_i $i = 0, \ldots, 4$ are some constants.

JHEP05(2019)117

As for $u \to +\infty$ the Kretschmann scalar for the right solution with (2.48)–(2.49) takes the form

$$K = \frac{21(16\mu_1 - 9k^2\mu_2)^4}{32(16-9k^2)^4} \left(\frac{C_1}{2E_1}\right)^{\frac{32}{16-9k^2}} \left(\frac{C_2}{2E_2}\right)^{\frac{18k^2}{9k^2-16}} e^{\frac{4(16\mu_1-9k^2\mu_2)}{16-9k^2}u}. \tag{A.39}$$

For the non-vacuum solutions (4.1) with (4.2)–(4.3) with (3.7) the Kretschmann scalar with reads $u \to u_{01} + \epsilon$

$$K \sim k_0(u-u_{01})^{\frac{64}{16-9k^2}} \sum_{i=0}^{4} c_i(\#(\alpha^1)^i)(u-u_{01})^{-i}, \tag{A.40}$$

while with $u \to +\infty$ is

$$\begin{aligned} K = {} & \frac{\left(4\alpha^1(9k^2-16)+27k^2\mu_2-48\mu_1\right)^2}{864(16-9k^2)^4} \left(\frac{C_1}{2E_1}\right)^{\frac{32}{16-9k^2}} \left(\frac{C_2}{2E_2}\right)^{\frac{18k^2}{9k^2-16}} e^{\frac{4(16\mu_1-9k^2\mu_2)}{16-9k^2}u} \\ & \cdot \left(304(\alpha^1)^2(16-9k^2)^2 + 168\alpha^1(9k^2-16)(16\mu_1-9k^2\mu_2) + 63(16\mu_1-9k^2\mu_2)^2\right). \end{aligned} \tag{A.41}$$

B The scalar field

We have the following relation for the scalar field

$$(\partial\phi)^2 = e^{-2C}\left(\frac{\partial\phi}{\partial u}\right)^2. \tag{B.1}$$

The dilaton solution defined for $u > u_{01}$ reads

$$\phi = \frac{9k}{9k^2-16}\log\left(\sqrt{\frac{C_2}{C_1}}\frac{\sinh(\mu_2(u-u_{02}))}{\sinh(\mu_1(u-u_{01}))}\right). \tag{B.2}$$

The derivative of the dilaton with respect to u-variable is

$$\frac{\partial\phi}{\partial u} = \frac{9k}{9k^2-16}\left(-\mu_1\frac{\cosh(\mu_1(u-u_{01}))}{\sinh(\mu_1(u-u_{01}))} + \mu_2\frac{\cosh(\mu_2(u-u_{02}))}{\sinh(\mu_2(u-u_{02}))}\right), \tag{B.3}$$

$$\left(\frac{\partial\phi}{\partial u}\right)^2 = \frac{81k^2}{(16-9k^2)^2}(\mu_1\coth(\mu_1(u-u_{01})) - \mu_2\coth(\mu_2(u-u_{02})))^2. \tag{B.4}$$

For the vacuum case one has

$$e^{-2C} = \left(\sqrt{\frac{C_1}{2E_1}}\sinh(\mu_1(u-u_{01}))\right)^{\frac{32}{16-9k^2}} \left(\sqrt{\frac{C_2}{2E_2}}\sinh(\mu_2(u-u_{02}))\right)^{\frac{18k^2}{9k^2-16}}. \tag{B.5}$$

The dilaton for $u \to u_{01} + \epsilon$ reads

$$\begin{aligned} (\partial\phi)^2 = {} & \frac{81k^2}{(16-9k^2)^2}((u-u_{01})^{-1} - \mu_2\coth(\mu_2(u_{01}-u_{02})))^2 \\ & \cdot \left(\sqrt{\frac{C_1}{2E_1}}\mu_1(u-u_{01})\right)^{\frac{32}{16-9k^2}} \left(\sqrt{\frac{C_2}{2E_2}}\sinh(\mu_2(u_{01}-u_{02}))\right)^{\frac{18k^2}{9k^2-16}}. \end{aligned} \tag{B.6}$$

Since $0 < k < 4/3$ the quantity $(\partial\varphi)^2$ has a good behaviour.

JHEP05(2019)117

In the limit $u \to +\infty$ the dilaton behaves as

$$(\partial\phi)^2 = \frac{81k^2}{(16-9k^2)^2}(\mu_1-\mu_2)^2\left(\frac{C_1}{2E_1}\right)^{\frac{16}{16-9k^2}}\left(\frac{C_2}{2E_2}\right)^{\frac{9k^2}{9k^2-16}} e^{\frac{2(16\mu_1-9k^2\mu_2)}{16-9k^2}u}. \tag{B.7}$$

The divergence disappears for $\mu_1 = \mu_2$ in the non-vacuum case.

C The superpotential in the UV

In this section, following the analysis of [14], we look at the superpotential in the neighborhood of the maximum of the potential, which is at $\phi \to -\infty$. Their analysis was done assuming that $V < 0$ so that the vacuum is asymptotically AdS, but we will show that their conclusions remain valid also in our case when $V \to 0$.

The equation that determines the superpotential in the vacuum is, in the domain wall coordinates,

$$V = \frac{4}{3}\left(\frac{dW}{d\phi}\right)^2 - \frac{64}{27}W^2\,, \tag{C.1}$$

$$A'(w) = -\frac{4}{9}W\,, \quad \phi'(w) = \frac{dW}{d\phi}\,. \tag{C.2}$$

These equations imply that $\frac{\phi'}{A'} = -\frac{9}{4}\frac{W'}{W}$. We want to solve it asymptotically in the UV, where $V = -|C_1|e^{2k\phi}$. There are two solutions: if one makes the ansatz that $W = \gamma e^{k\phi}$, substituting in the equation gives

$$\gamma^2 = \frac{27|C_1|}{4(16-9k^2)}\,, \tag{C.3}$$

so the solution is uniquely determined. This is the "regular" solution in the terminology of [14], and on this solution $X = \frac{\phi'}{3A'} \to -\frac{3k}{4}$.

Another solution is obtained by assuming that the superpotential terms are dominant in (C.2), so one can set $V = 0$ and finds $W = ce^{-4\phi/3}$. Since $k < 4/3$, $W^2 \gg V$ so the assumption is self-consistent. In this case c is arbitrary, so there is a 1-parameter family of solutions for which $X \to 1$. These are singular solutions.

The plots in figure 9 show that these two cases correspond to the asymptotics of the right solutions, in the UV and IR respectively. We can check this explicitly by computing the superpotential from the asymptotics of the solution given in (3.2)–(3.3). In these formulas the coordinate u is not the domain wall coordinate, which is obtained by $dw = e^{4A}du$. The superpotential is then $W = -\frac{9}{4}e^{-4A}A'(u)$. For convenience we set $u_{01} = 0$. The UV asymptotics, for $u \sim 0$, are

$$A \sim -\frac{4}{16-9k^2}\log u + A_0\,, \tag{C.4}$$

$$\phi \sim \frac{9k}{16-9k^2}\log u + \phi_0\,, \tag{C.5}$$

JHEP05(2019)117

where

$$A_0 = -\frac{4}{16-9k^2}\log\left(\sqrt{\frac{|C_1|}{2|E|}}\mu_1\right) + \frac{9k^2}{4(16-9k^2)}\log\left(\sqrt{\frac{|C_2|}{2|E|}}\sinh(-\mu_2 u_{02})\right), \tag{C.6}$$

$$\phi_0 = \frac{9k}{16-9k^2}\log\left(\sqrt{\frac{|C_1|}{|C_2|}}\frac{\mu_1}{\sinh(-\mu_2 u_{02})}\right). \tag{C.7}$$

Then

$$W = -\frac{9}{4}e^{-4A}A' = \frac{9}{16-9k^2}e^{-4A_0}e^{\frac{9k^2}{16-9k^2}\log u} = \frac{9}{16-9k^2}e^{-4A_0-k\phi_0}e^{k\phi} \tag{C.8}$$

and a rather tedious computation shows that the coefficient is equal to γ in (C.3), so the dependence on all the parameters of the solution cancels out.

At $u \to \infty$ we have the asymptotics

$$A \sim -\frac{\mu_1}{4+3k}u + A_\infty\,, \tag{C.9}$$

$$\phi \sim -\frac{3\mu_1}{4+3k}u + \phi_\infty\,, \tag{C.10}$$

where

$$A_\infty = -\frac{4}{16-9k^2}\log\sqrt{\frac{|C_1|}{8|E|}} + \frac{9k^2}{4(16-9k^2)}\left(-\mu_2 u_{02} + \log\sqrt{\frac{|C_2|}{8|E|}}\right), \tag{C.11}$$

$$\phi_0 = \frac{9k}{16-9k^2}\left(\mu_2 u_{02} + \log\sqrt{\frac{|C_1|}{|C_2|}}\right). \tag{C.12}$$

Then

$$W = \frac{9\mu_1}{4(4+3k)}e^{-4A_\infty}e^{\frac{4\mu_1}{4+3k}u} = \frac{9\mu_1}{4(4+3k)}e^{-4A_\infty+\frac{4}{3}\phi_\infty}e^{-\frac{4}{3}\phi}\,. \tag{C.13}$$

In this case there is no cancellation and the coefficient depends on the parameters of the solution, as expected.

The analysis of [14] then leads to the conclusion that all the flows that end in the singular IR solution are not acceptable because they cannot be regularized by a small horizon. Indeed we see that when we turn on the temperature, we have no regular flow that ends in the vicinity of $X = 1$. The only regular vacuum flow is the one that ends at $X = 0$, shown in figure 9C, which ends at a different extremum of the potential; we do not need to analyse it in detail since the asymptotics are those of AdS.

JHEP05(2019)117

References

[1] J. de Boer, E.P. Verlinde and H.L. Verlinde, *On the holographic renormalization group*, *JHEP* **08** (2000) 003 [hep-th/9912012] [INSPIRE].

[2] H.J. Boonstra, K. Skenderis and P.K. Townsend, *The domain wall/QFT correspondence*, *JHEP* **01** (1999) 003 [hep-th/9807137] [INSPIRE].

[3] M. Bianchi, D.Z. Freedman and K. Skenderis, *Holographic renormalization*, *Nucl. Phys.* **B 631** (2002) 159 [hep-th/0112119] [INSPIRE].

[4] K. Skenderis, *Lecture notes on holographic renormalization*, *Class. Quant. Grav.* **19** (2002) 5849 [hep-th/0209067] [INSPIRE].

[5] I. Heemskerk and J. Polchinski, *Holographic and Wilsonian Renormalization Groups*, *JHEP* **06** (2011) 031 [arXiv:1010.1264] [INSPIRE].

[6] T. Faulkner, H. Liu and M. Rangamani, *Integrating out geometry: Holographic Wilsonian RG and the membrane paradigm*, *JHEP* **08** (2011) 051 [arXiv:1010.4036] [INSPIRE].

[7] S.-S. Lee, *Quantum Renormalization Group and Holography*, *JHEP* **01** (2014) 076 [arXiv:1305.3908] [INSPIRE].

[8] E. Kiritsis, F. Nitti and L. Silva Pimenta, *Exotic RG Flows from Holography*, *Fortsch. Phys.* **65** (2017) 1600120 [arXiv:1611.05493] [INSPIRE].

[9] H.A. Chamblin and H.S. Reall, *Dynamic dilatonic domain walls*, *Nucl. Phys.* **B 562** (1999) 133 [hep-th/9903225] [INSPIRE].

[10] U. Gürsoy, M. Järvinen and G. Policastro, *Late time behavior of non-conformal plasmas*, *JHEP* **01** (2016) 134 [arXiv:1507.08628] [INSPIRE].

[11] P. Betzios, U. Gürsoy, M. Järvinen and G. Policastro, *Quasinormal modes of a strongly coupled non-conformal plasma and approach to criticality*, *Phys. Rev.* **D 97** (2018) 081901 [arXiv:1708.02252] [INSPIRE].

[12] A.N. Leznov and M.V. Saveliev, *Group theoretical methods for integration of nonlinear dynamical systems*, Nauka, Moscow Russia (1985).

[13] A.M. Perelomov, *Integrable systems of Classical Mechanics and Lie Algebras*, Nauka, Moscow Russia (1990).

[14] U. Gürsoy, E. Kiritsis, L. Mazzanti and F. Nitti, *Holography and Thermodynamics of* $5D$ *Dilaton-gravity*, *JHEP* **05** (2009) 033 [arXiv:0812.0792] [INSPIRE].

[15] B. Gouteraux and E. Kiritsis, *Generalized Holographic Quantum Criticality at Finite Density*, *JHEP* **12** (2011) 036 [arXiv:1107.2116] [INSPIRE].

[16] D.Z. Freedman, S.S. Gubser, K. Pilch and N.P. Warner, *Renormalization group flows from holography: Supersymmetry and a c-theorem*, *Adv. Theor. Math. Phys.* **3** (1999) 363 [hep-th/9904017] [INSPIRE].

[17] E. Kiritsis, W. Li and F. Nitti, *Holographic RG flow and the Quantum Effective Action*, *Fortsch. Phys.* **62** (2014) 389 [arXiv:1401.0888] [INSPIRE].

[18] V.R. Gavrilov, V.D. Ivashchuk and V.N. Melnikov, *Integrable pseudo-Euclidean Toda-like systems in multidimensional cosmology with multicomponent perfect fluid*, *J. Math. Phys.* **36** (1995) 5829 [INSPIRE].

JHEP05(2019)117

[19] R. Endo, *Heat kernel for spin 3/2 Rarita-Schwinger field in general covariant gauge*, *Class. Quant. Grav.* **12** (1995) 1157 [hep-th/9407019] [INSPIRE].

[20] V.D. Ivashchuk, V.N. Melnikov and A.B. Selivanov, *Cosmological solutions in multidimensional model with multiple exponential potential*, *JHEP* **09** (2003) 059 [hep-th/0308113] [INSPIRE].

[21] A.A. Golubtsova and V.D. Ivashchuk, *Exact solutions in gravity with a σ-model source*, *Gen. Rel. Grav.* **44** (2012) 2571 [arXiv:1204.0091] [INSPIRE].

[22] S.S. Gubser, *Curvature singularities: The Good, the bad and the naked*, *Adv. Theor. Math. Phys.* **4** (2000) 679 [hep-th/0002160] [INSPIRE].

[23] I. Papadimitriou, *Holographic Renormalization of general dilaton-axion gravity*, *JHEP* **08** (2011) 119 [arXiv:1106.4826] [INSPIRE].

[24] U. Gürsoy, E. Kiritsis, F. Nitti and L. Silva Pimenta, *Exotic holographic RG flows at finite temperature*, *JHEP* **10** (2018) 173 [arXiv:1805.01769] [INSPIRE].

[25] H. Lü, C.N. Pope, E. Sezgin and K.S. Stelle, *Dilatonic p-brane solitons*, *Phys. Lett.* **B 371** (1996) 46 [hep-th/9511203] [INSPIRE].

[26] S.H. Hendi, A. Sheykhi and M.H. Dehghani, *Thermodynamics of higher dimensional topological charged AdS black branes in dilaton gravity*, *Eur. Phys. J.* **C 70** (2010) 703 [arXiv:1002.0202] [INSPIRE].

JHEP05(2019)117